Electronic Supplementary Material (ESI) for Chemical Science.
This journal is © The Royal Society of Chemistry 2020

Self-Assembly of Reversed Bilayer Vesicles through Pnictogen Bonding: Water-stable Supramolecular Nanocontainers for Organic Solvents

*Shiva Moaven, Brandon T. Watson, Shelby B. Thompson, Veronica J. Lyons, Daniel K. Unruh, Dominick J. Casadonte, Dimitri Pappas, and Anthony F. Cozzolino**

Electronic Supplementary Information

Department of Chemistry and Biochemistry, Texas Tech University, Box 1061, Lubbock, Texas 79409-1061, United States

Table of Contents

S1 Experimental Details

S1.1 General Methods

The starting materials, antimony(III) *tert*-butoxide was prepared according to our previous report.[1] 1,1,1-trimethylolpropane (99%, Merck), 4-touluenesulfonyl chloride (99%, Acros Organics), potassium thiocyanate (99%, Acros Organics), lithium aluminum hydride, were used as purchased. Pyridine (Fisher, ACS grade), and acetonitrile (99.5%, Sigma-Aldrich) were used without further purification. Anhydrous tetrahydrofuran, Diethyl ether, and hexanes were obtained by passing HPLC grade tetrahydrofuran and diethyl ether and ACS grade hexanes over a bed of activated molecular sieves in a commercial (LC Technologies Solutions Inc.) solvent purification system (SPS). Deuterated solvents were purchased from Cambridge Isotopes Laboratory. Air sensitive manipulations were performed in a N_2 purged inert atmosphere box (LC Technology Solutions Inc.). All NMR spectra were collected on a JEOL ECS 400 MHz NMR spectrometer, unless stated, all data was collected at 21 °C. All IR spectra were obtained using a Nicolet iS 5 FT-IR spectrometer equipped with a Specac Di Quest ATR accessory. All cyclic voltammetry analyses were performed using a BASi Epsilon potensiostat/galvanostat instrument.

S1.2 Synthesis

S1.2.1 Preparation of 1,1,1-Trimercaptomethylpropane, $(HSCH_2)_3CC_2H_5$ ($H_3\mathbf{1}_{Et}$)

Following the previously reported procedure[2] 1,1,1-Trimercaptomethylpropane was prepared, as shown in Scheme S1, in three steps. In an Erlenmeyer flask, 14.09 g (107 mmol) of 1,1,1-trimethylolpropane was dissolved in 50 mL of pyridine and the solution was cooled down to 0 °C. A slurry of 4-tulenesulfonylchloride (71.68 g, 376 mmol) in 25 mL of pyridine was added to the cold solution over the course of 2 hours. The mixture was allowed to warm up to room temperature and stirred overnight. The milky mixture was poured onto a mixture of crushed ice and 100 mL of

concentrated hydrochloric acid. After addition a white solid precipitated out. The crude solid was filtered and later recrystallized from 150 mL of acetone stored at −25 °C for 12 hours. The recrystallized product **3** was filtered and washed with 100 mL of ethanol, final mass 58.958 g (98.8 mmol), yield 92.3%. ^{1}H NMR (400 MHz, DMSO-d_6, δ): 0.49 (t, *J*=7.56 Hz, 3 H), 1.20 (q, *J*=7.33 Hz, 2 H), 2.43 (s, 9H), 3.75 (s, 6H), 7.47 (d, *J*=8.24 Hz, 6 H) 7.69 (d, *J*=8.24 Hz, 6 H). ^{13}C{^{1}H} NMR (100.6 MHz, DMSO-d_6, δ): 6.23, 20.93, 21.15, 41.40, 67.70, 127.64, 130.26, 131.41, 145.30. FTIR (ATR, cm^{-1}) 3050 (w, Csp^2–H), 2962 (m, Csp^3–H), 1596 (s, C=C), 1354 and 1173 (s, C–SO_2–OC).

Dry DMF (35 mL) was added to a solid mixture of **3** (26.00 g, 43.5 mmol) and potassium thiocyanate (55.40 g, 570 mmol). The mixture was slowly brought to reflux, where it became a homogeneous solution, and left to stir for 5 hours. After the allotted time, the mixture was poured onto 600 mL of water and stored at 4 °C for 18 hours. The tan precipitate **4** was filtered and washed with 100 mL of cold ethanol:diethyl ether (1:1), and 50 mL of cold diethyl ether, final mass 4.484 g (17.4 mmol), yield 40.0%. ^{1}H NMR (400 MHz, $CDCl_3$, δ): 1.00 (t, *J*=7.56 Hz, 3 H), 1.78 (q, *J*=7.33 Hz, 2 H), , 3.25 (s, 6H). ^{13}C{^{1}H} NMR (100.6 MHz, $CDCl_3$, δ): 7.82, 26.86, 38.42, 44.73, 111.25. FTIR (ATR, cm^{-1}) 2983 (s, Csp^3–H), 2149 (vs, C≡N).

A 4.10 g (15.9 mmol) sample of **4** was suspended in anhydrous diethyl ether. The mixture was cooled down to 0 °C in an ice-water bath. Through an addition funnel, 10.0 g (263 mmol) of lithium aluminum hydride was added slowly over 2 hours. After the addition was over, the solution was allowed to warm up to room temperature and then it was refluxed for 16 hours. The mixture was cooled down to 0 °C and the excess lithium aluminum hydride was quenched with saturated aqueous ammonium chloride solution. The product was extracted with diethyl ether (50 mL × 3). After the solvent was evaporated under reduced pressure 2.862 g (15.7 mmol) of a yellow oil

(H_3**1**$_{Et}$) with pungent odor was recovered, yield 98.7%. ^{1}H NMR (400 MHz, $CDCl_3$, δ): 0.49 (t, *J*=7.56 Hz, 3 H), 1.20 (q, *J*=7.33 Hz, 2 H), 3.75 (s, 6H). ^{13}C NMR (100.6 MHz, $CDCl_3$, δ): 7.78, 24.96, 28.70, 41.51. FTIR (ATR, cm^{-1}) 2960 (s, C*sp*^{3}–H), 2552 (m, S–H), 713 and 677 (m, C–S).

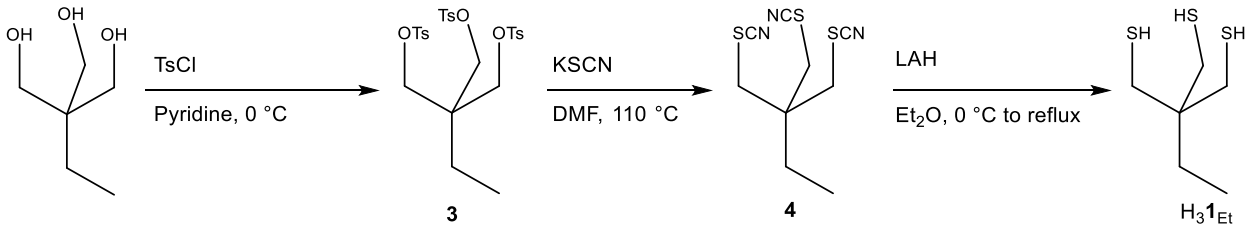

Scheme S1. Synthetic route for preparation of H_3**1**$_{Et}$.

S1.2.2 Preparation of antimony (III) 1,1,1-trimethylmercaptopropane (Sb-**1**$_{Et}$, $Sb(SCH_2)_3CC_2H_5$)

In 5 mL of anhydrous hexanes 182 mg (0.999 mmol) of H_3**1**$_{Et}$ was dissolved. At ~21 °C, 341 mg of antimony tris-*tert*-butoxide (0.999 mmol) dissolved in 2 mL of anhydrous hexanes was added and to the solution with stirring. A milky white precipitate formed immediately. The solid was filtered in ambient conditions and 262 mg of white solid was recovered, yield 87.1%. ^{1}H NMR (400 MHz, DMSO-*d6*, δ): 0.79 (t, *J*=7.32 Hz, 3 H), 1.28 (q, *J*=6.96 Hz, 2 H), 2.98 (s, 6H). ^{13}C NMR (100.6 MHz, DMSO-*d6*, δ): 8.61, 31.28, 37.69, 38.26. FTIR (ATR, cm^{-1}) 2957 (s, C*sp*^{3}–H), 672, 622, 520 (m, C–S).

S1.3 Crystallography

Single crystals of compound Sb-$\mathbf{1}_{Et}$ were obtained by sonicating the amorphous solid recovered from the reaction mixture in acetonitrile followed by slow evaporation of the resulting suspension. For compound Sb-$\mathbf{1}_{Et}$ data was collected on a Bruker PLATFORM three circle diffractometer equipped with an APEX II CCD detector and operated at 1500 W (50kV, 30 mA) to generate (graphite monochromated) Mo Kα radiation (λ = 0.71073 Å). Crystals were transferred from the vial and placed on a glass slide in polyisobutylene. A Zeiss Stemi 305 microscope was used to identify a suitable specimen for X-ray diffraction from a representative sample of the material. The crystal and a small amount of the oil were collected on a MiTiGen cryoloop and transferred to the instrument where it was placed under a cold nitrogen stream (Oxford) maintained at 100K throughout the duration of the experiment. The sample was optically centered with the aid of a video camera to insure that no translations were observed as the crystal was rotated through all positions.

A unit cell collection was carried out followed by the collection of a sphere of data. Omega scans were carried out with a 10 sec/frame exposure time and a rotation of 0.50° per frame. After data collection, the crystals were measured for size, morphology, and color.

Intensity data were corrected for Lorentz, polarization, and background effects using the Bruker program APEX 3. A semi-empirical correction for adsorption was applied using the program *SADABS*.[3] The *SHELXL-2014* series of programs were used for the solution and refinement of the crystal structure.[4] Hydrogen atoms bound to carbon atoms were located in the difference Fourier map and were geometrically constrained using the appropriate AFIX commands. The Z' value for the structure was 2.

Table S1. Crystal data and structure refinement for Sb-**1**$_{Et}$.

	Sb-**1**$_{Et}$
Crystal Color	colorless
Crystal Habit	block
Empirical formula	$C_6H_{11}S_3Sb$
Formula weight	301.08
Temperature	100(2) K
Wavelength	0.71073 A
Crystal system	Monoclinic
Space group	$P2_1/n$
Unit cell dimensions	a = 7.5797(7) Å α = 90 °
	b = 9.1057(9) Å β = 95.2180(10) °
	c = 27.371(3) Å γ = 90 °
Volume	1881.3(3) Å^3
Z	8
Calculated density	2.126 Mg/m^3
Absorption coefficient	3.526 mm^{-1}
F(000)	1168
Crystal size	0.245 × 0.120 × 0.120 mm
Theta range for data collection	1.494 to 27.168 °.
Limiting indices	-9≤ h ≤9, -11≤ k ≤11, -35≤ l ≤35
Reflections collected / unique	21518 / 4176 [R(int) = 0.0253]
Completeness to theta = 25.242°	100.0 %
Refinement method	Full-matrix least-squares on F^2
Data / restraints / parameters	4176 / 0 / 183
Goodness-of-fit on F^2	1.069
Final R indices [I>2sigma(I)]	R1 = 0.0178, wR2 = 0.0412
R indices (all data)	R1 = 0.0212, wR2 = 0.0429
Largest diff. peak and hole	0.416 and -0.831 e.A^{-3}

S1.4 Computational Methods

Calculations were performed using the ORCA 4.0 quantum chemistry program package from the development team at the Max Planck Institute for Bioinorganic Chemistry.[6] The starting geometry for optimization of Sb-$\mathbf{1}_{Et}$ was based on the solved crystal structure of Sb-$\mathbf{1}_{Et}$. In order to allow for the comparison with the energy of different dimers within the alkoxide bilayer[1] only the position of the hydrogen atoms where optimized in these cases starting from the solved crystal structures of all supramolecular structures (Sb-$\mathbf{1}_{Et}$, Sb-$\mathbf{2}_{Pr}$, As-$\mathbf{1}_{Et}$). The alkyl groups were replaced with a hydrogen atom on all (now Sb-$\mathbf{1}_{H}$, Sb-$\mathbf{2}_{H}$, As-$\mathbf{1}_{H}$) in order to have a proper comparison between the results. Monomers were allowed to optimize completely. All calculations were carried out using the Zero-Order Regular Approximation (ZORA).[7,8] For geometry optimizations, frequencies, and thermochemistry the B97-D3[9] functional and def2-TZVPP[10,11] with SARC/J basis sets[12] were used for hydrogen atoms and all other atoms respectively. Spin-restricted Kohn– Sham determinants[13] were chosen to describe the closed shell wavefunctions, employing the RI approximation[14] and the tight SCF convergence criteria provided by ORCA. The basis set superposition error (BSSE) was corrected using the Boys and Bernardi procedures.[15] Molecular electrostatic potential (ESP) mapping was performed on the 0.001 isosurface of the electron density using the Multiwfn program. [16,17] All visualizations of ESP maps were performed with the Gabedit graphical interface software.[18] The cartesian coordinates of the geometry optimized molecules and supramolecules are provided as .xyz files in a .zip file.

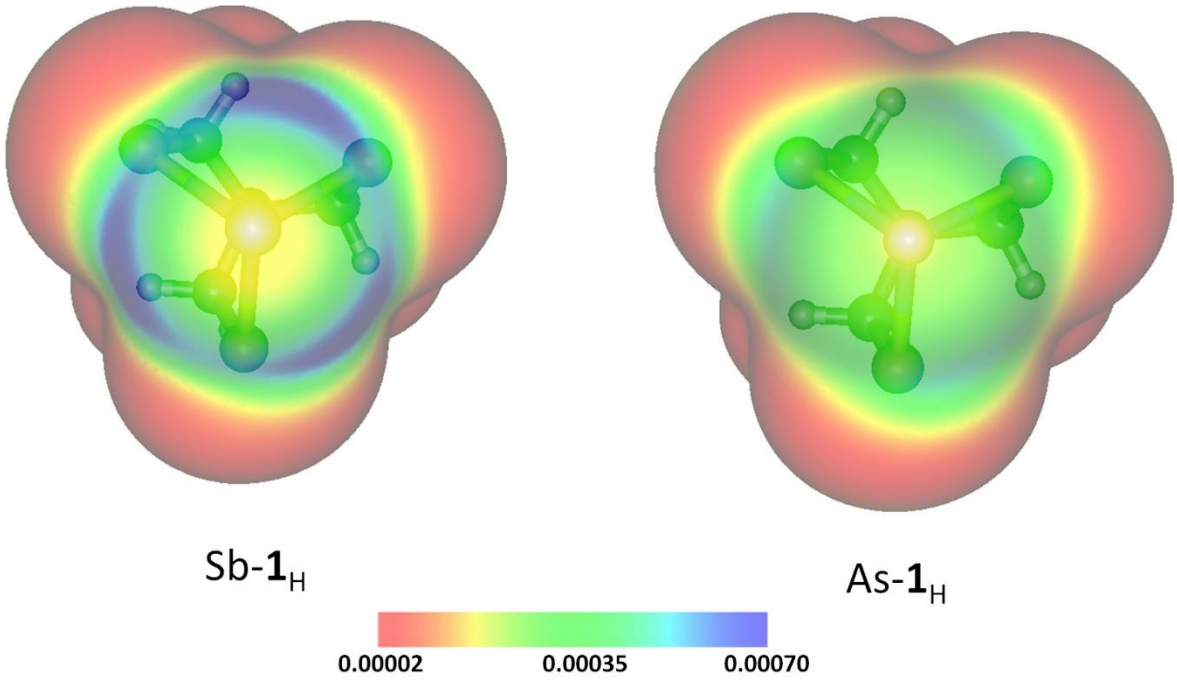

Fig. S1. Fukui function from above of Sb-$\mathbf{1}_H$ (left) and As-$\mathbf{1}_H$ (right) from top view mapped on the electron density surface (0.001 au isosurface). Blue regions depict areas susceptible to nucleophilic attack.

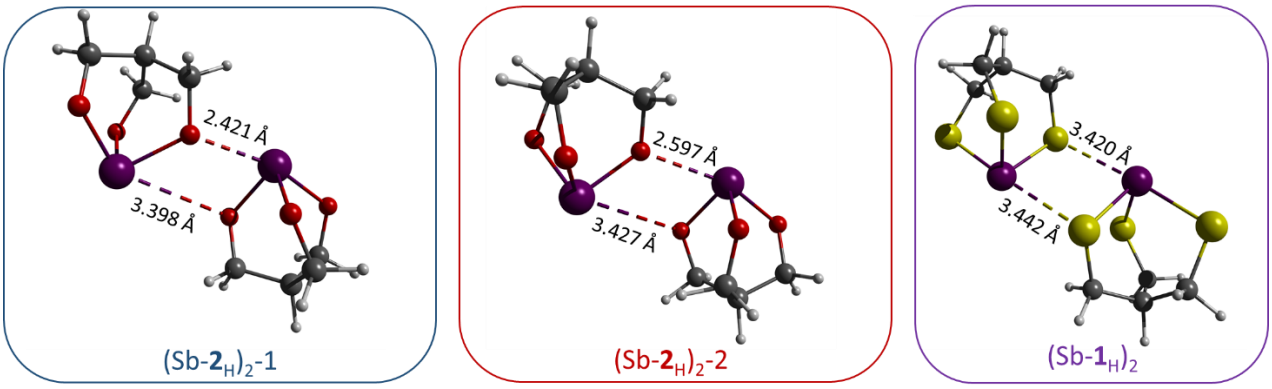

Fig. S2. Dimers of Sb-$\mathbf{2}_H$ compound (left and middle) and Sb-$\mathbf{1}_H$ dimer (right) with optimized hydrogen positions.

Table S2. Summary of the energetics for gas phase monomers and dimers of alkoxide and thiolate compounds along with dimerization energies (ΔE_D) with and without a dispersion contribution.

Compound	E (Eh)	Dispersion correction (Eh)	BSSE correction (kJ/mol)	ΔE_D (kJ/mol) [a]	$\Delta E_{D+disp.}$ (kJ/mol) [b]
Sb-**2**$_H$	−7075.990224	−0.076177135			
(Sb-**2**$_H$)-1	−14152.00272	−0.167572802	7.13	−51.36	−91.31
(Sb-**2**$_H$)-2	−14152.00406	−0.167012384	6.76	−55.22	−93.71
Sb-**1**$_H$	−7932.02515	−0.065254776			
(Sb-**1**$_H$)$_2$	−15864.06723	−0.151665823	3.13	−41.31	−96.86

(a) = Dimerization energy + BSSE correction

(b) = Dimerization energy +BSSE correction + Dispersion corrections

S1.5 Dynamic Light Scattering (DLS) Method

Samples were characterized using a Nanotrac Model NPA250 (Microtrac Inc.). All samples were prepared in acetone under ambient conditions. Solvent, time, probe amplitude, and concentration effect on the formation of the vesicles were studied. Four different concentrations (0.50, 0.25, 0.10, and 0.05 mM) of Sb-$\mathbf{1}_{Et}$ were prepared in 40 mL scintillation vials. The ultrasonic probe was dipped inside 20 mL solutions of Sb-$\mathbf{1}_{Et}$ and sonicated for 2, 5, and 10 minutes. All DLS experiments were performed in triplicate. Following sonication the laser was dipped into the solution. For each sample, two 60 second scans were performed. The data was processed with microtrac FLEX 10.3.14 and the size distribution, in percent, of the particles was plotted as a function of the size of the particles in nanometers after averaging the three independent trials.

S1.6 Transmission Electron Microscopy (TEM) Method

Based on the DLS results, 0.3, 0.6, 1.5, and 3.0 mg of Sb-$\mathbf{1}_{Et}$ were dispersed in 20 mL of acetone and sonicated for 5 minutes under ambient conditions. A drop of the prepared solution was cast on a 200 mesh carbon-coated copper grid (Ted Pella, inc.) and excess solvent was removed by absorbing it with a filter paper placed under the grid. Samples were characterized with a Hitachi H-7650 scanning transmission electron microscope. Samples were studied under 60 keV accelerating voltage. Image capturing and size measurements were performed with the AMT imaging software.

S1.7 Scanning Electron Microscopy (SEM) Method

Based on the DLS results, 0.3, 0.6, 1.5, and 3.0 mg of Sb-$\mathbf{1}_{Et}$ was dispersed in 20 mL of acetone and sonicated for 5 minutes under ambient conditions. A drop of the prepared solution was cast on a 200 mesh carbon coated copper grid (Ted Pella, inc.) and excess solvent was removed by absorbing it with a filter paper placed under the grid. Then grid was placed on double sided carbon

adhesive tape. The sample was coated with iridium and the morphology of the specimen was imaged with a Hitachi S-4300 scanning electron microscope.

S1.8 Fluorescence Microscopy

Vesicles containing rhodamine B dye (RhB) were imaged using an Olympus IX51 inverted microscope with a 60×, 0.67 NA dry objective. An epifluorescent light source with a wavelength of 508 nm was used to excite the particles. The camera used for imaging was a Zyla 5.5 sCMOS with a pixel size of 6.5 μm × 6.5 μm or a Thorlabs Quantulux sCMOS with a pixel size of 5 μm × 5 μm. For fluorescence imaging a drop of the dialyzed sample was drop cast on a glass slide.

Vesicles containing 6-carboxyfluorecein dye (6-FAM) were imaged using a Nikon Ti2-A E20L80 inverted microscope with a 20×, 0.75 NA dry objective. An epifluorescent light source with a wavelength of 495 nm was used to excite the particles. The camera used for imaging was a Zyla 5.5 sCMOS with a pixel size of 6.5 μm × 6.5 μm or a Thorlabs Quantulux sCMOS with a pixel size of 5 μm × 5 μm. For fluorescence imaging a drop of the dialyzed sample was drop cast on a glass slide.

Vesicles containing acridone based dye (Ac) were imaged using an Olympus IX71 inverted microscope with a 20×, 0.50 dry objective. An epifluorescent light source with a wavelength of 365 nm was used to excite the particles, for which a blue-purple fluorescence was observed. The camera used for imaging was a Thorlabs Quantulux sCMOS with a pixel size of 5 μm × 5 μm. For fluorescence imaging a drop of the dialyzed sample was drop cast on a glass slide.

S2 Spectroscopic Data

S2.1 ^{1}H NMR

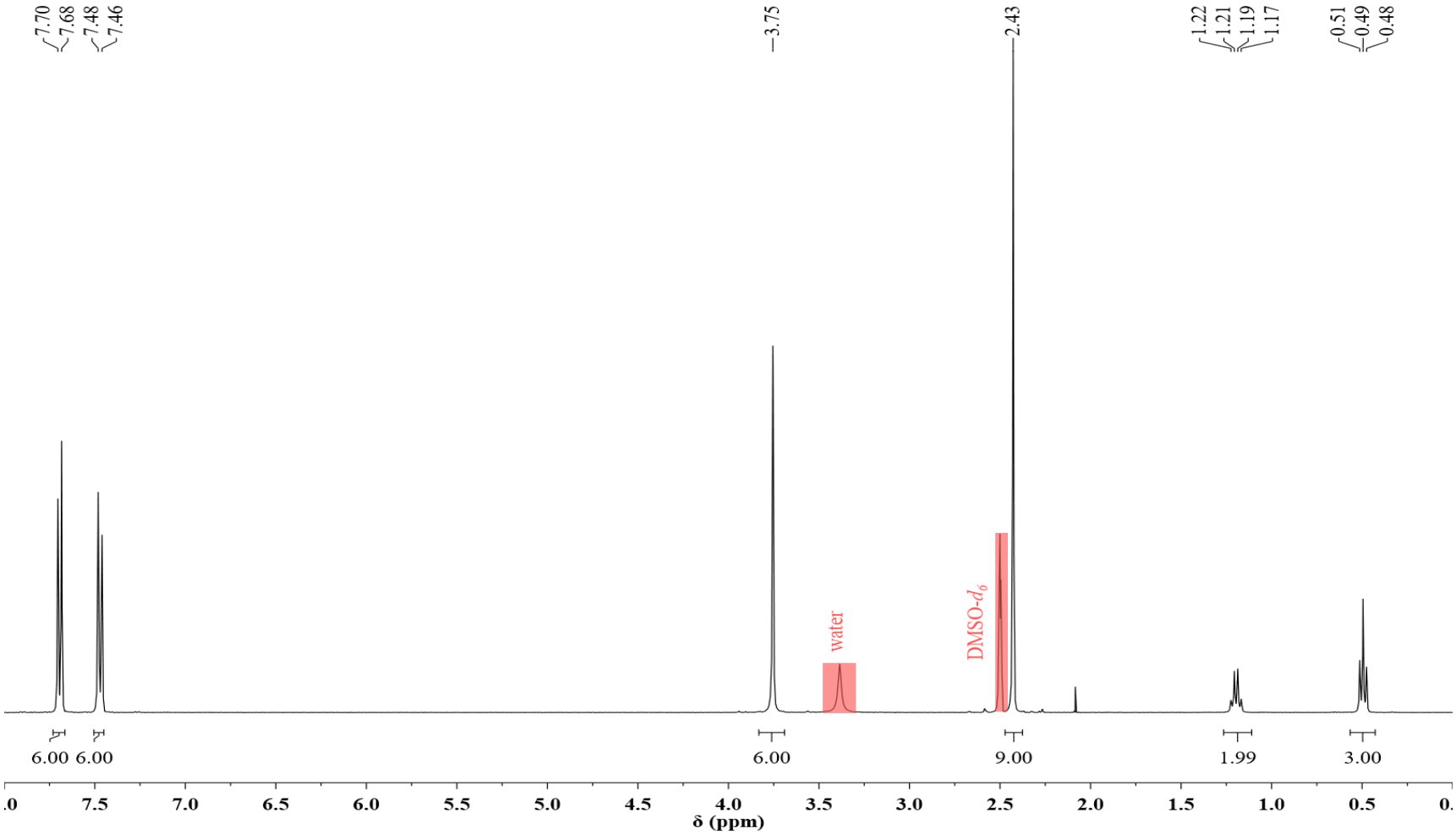

Fig. S3. ^{1}H NMR of **3** in DMSO-*d6*.

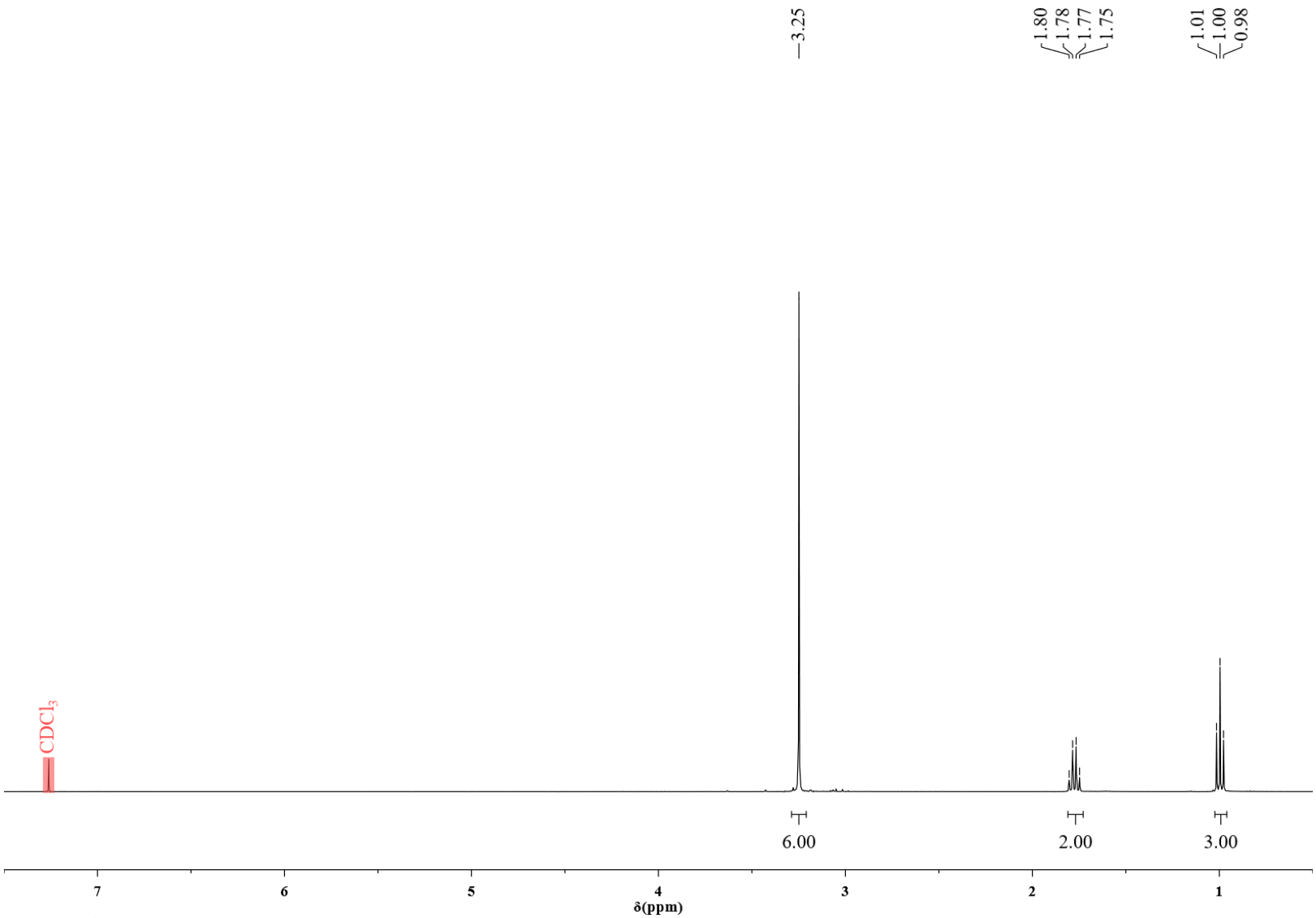

Fig. S4. ^{1}H NMR of **4** in $CDCl_3$.

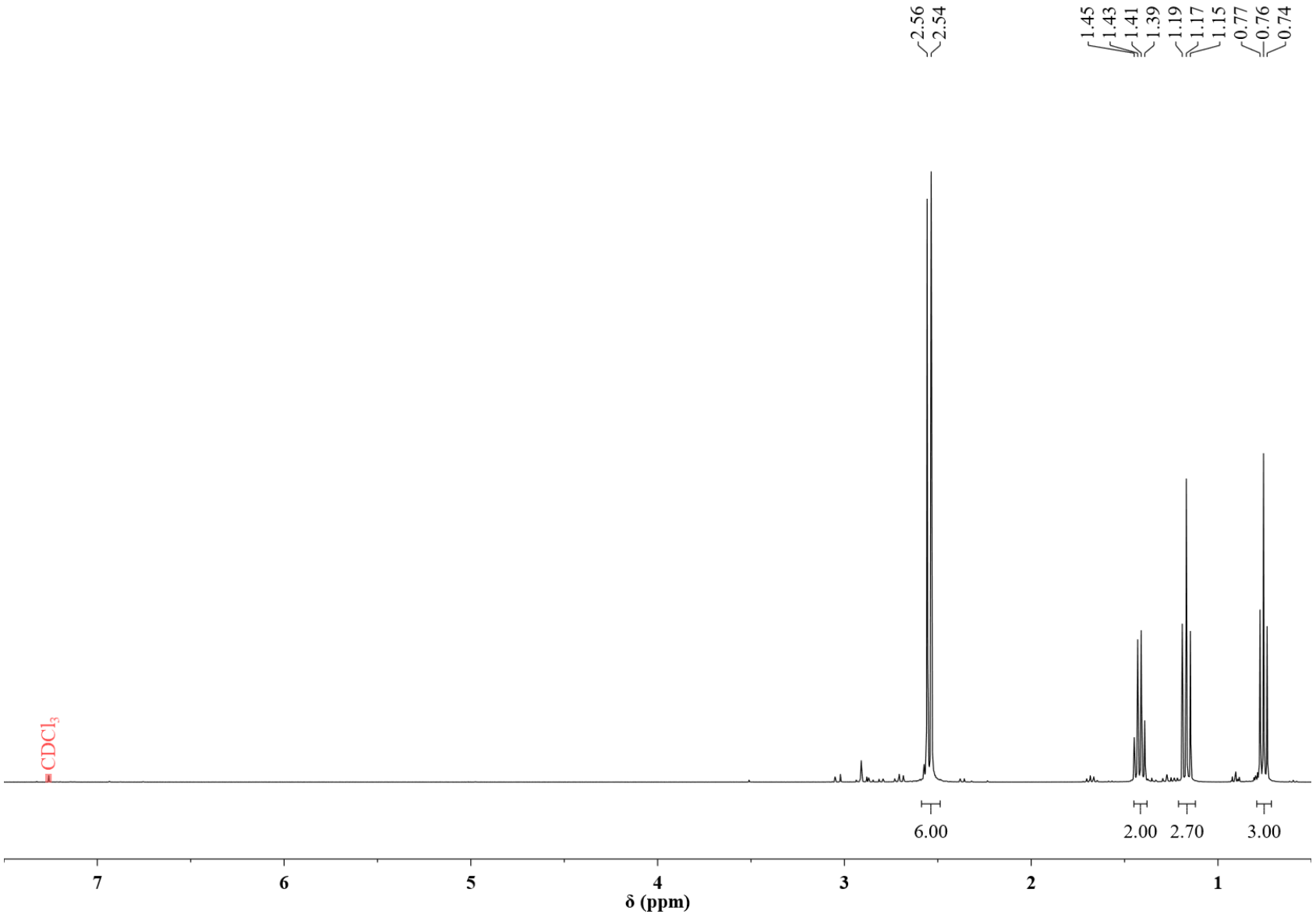

Fig. S5. ^{1}H NMR $H_3\mathbf{1}_{Et}$ in $CDCl_3$.

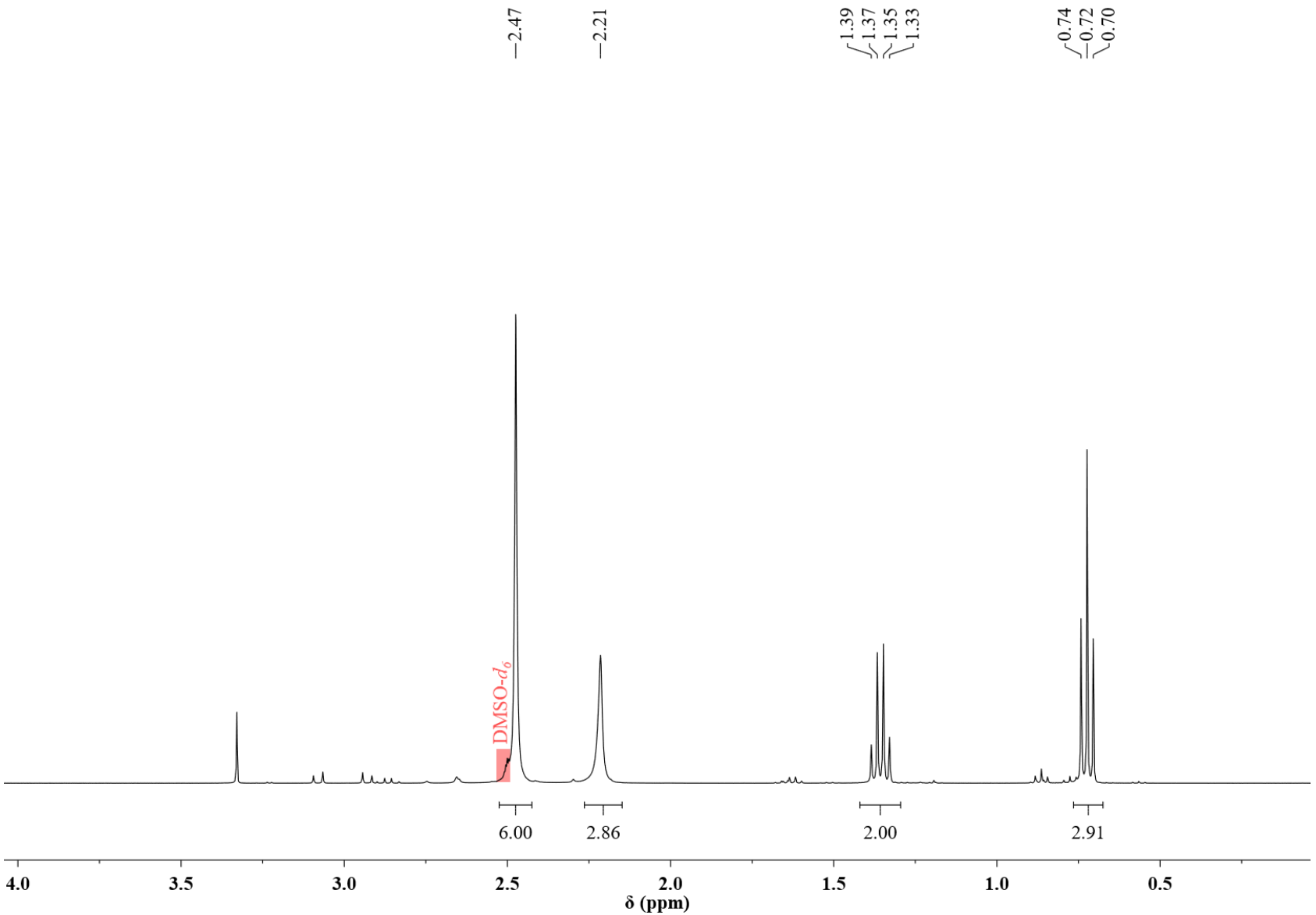

Fig. S6. ^{1}H NMR of H_3**1**$_{Et}$ in DMSO-*d6*.

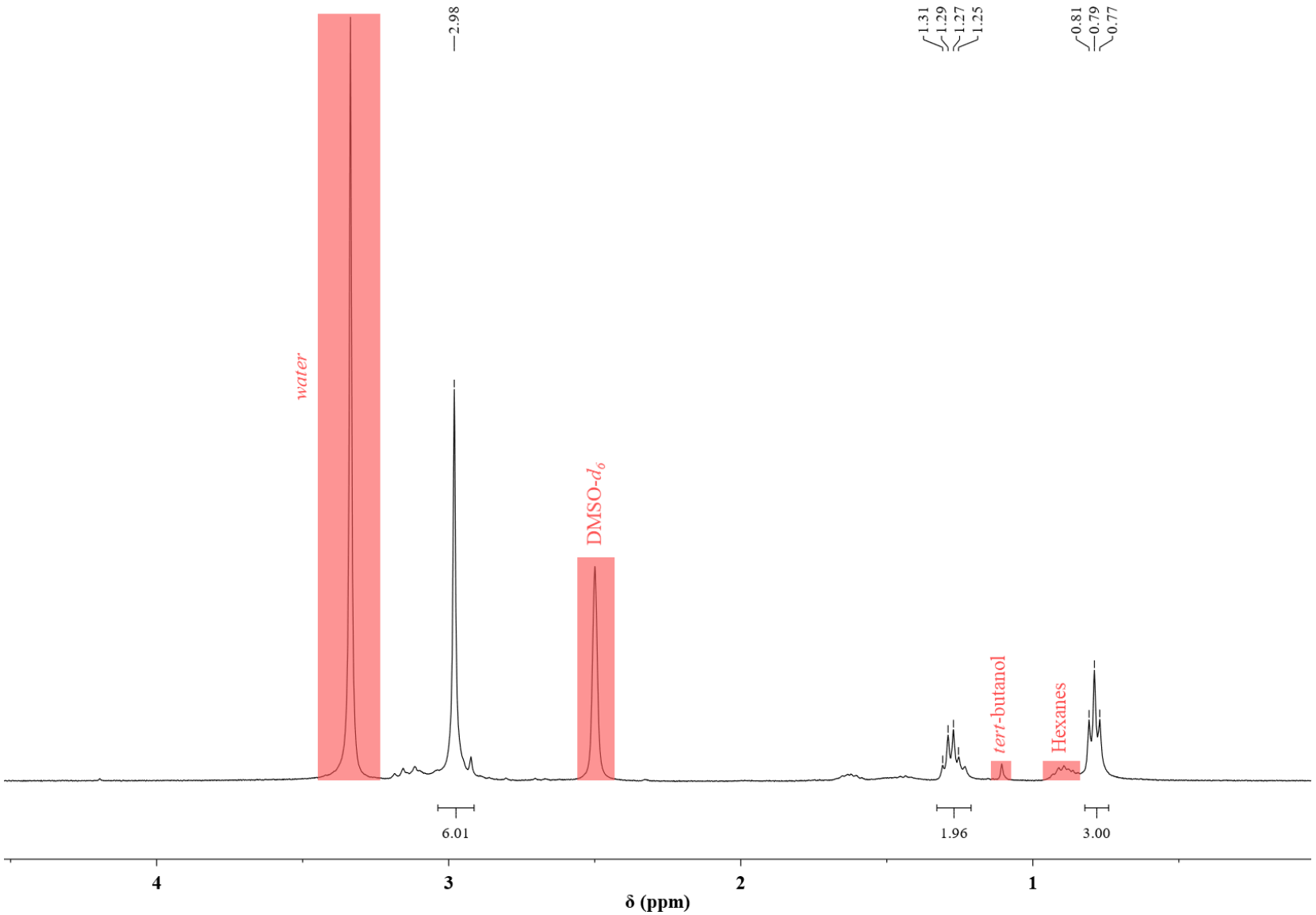

Fig. S7. ^{1}H NMR of Sb-**1**$_{Et}$ in DMSO-*d6* at 60 °C.

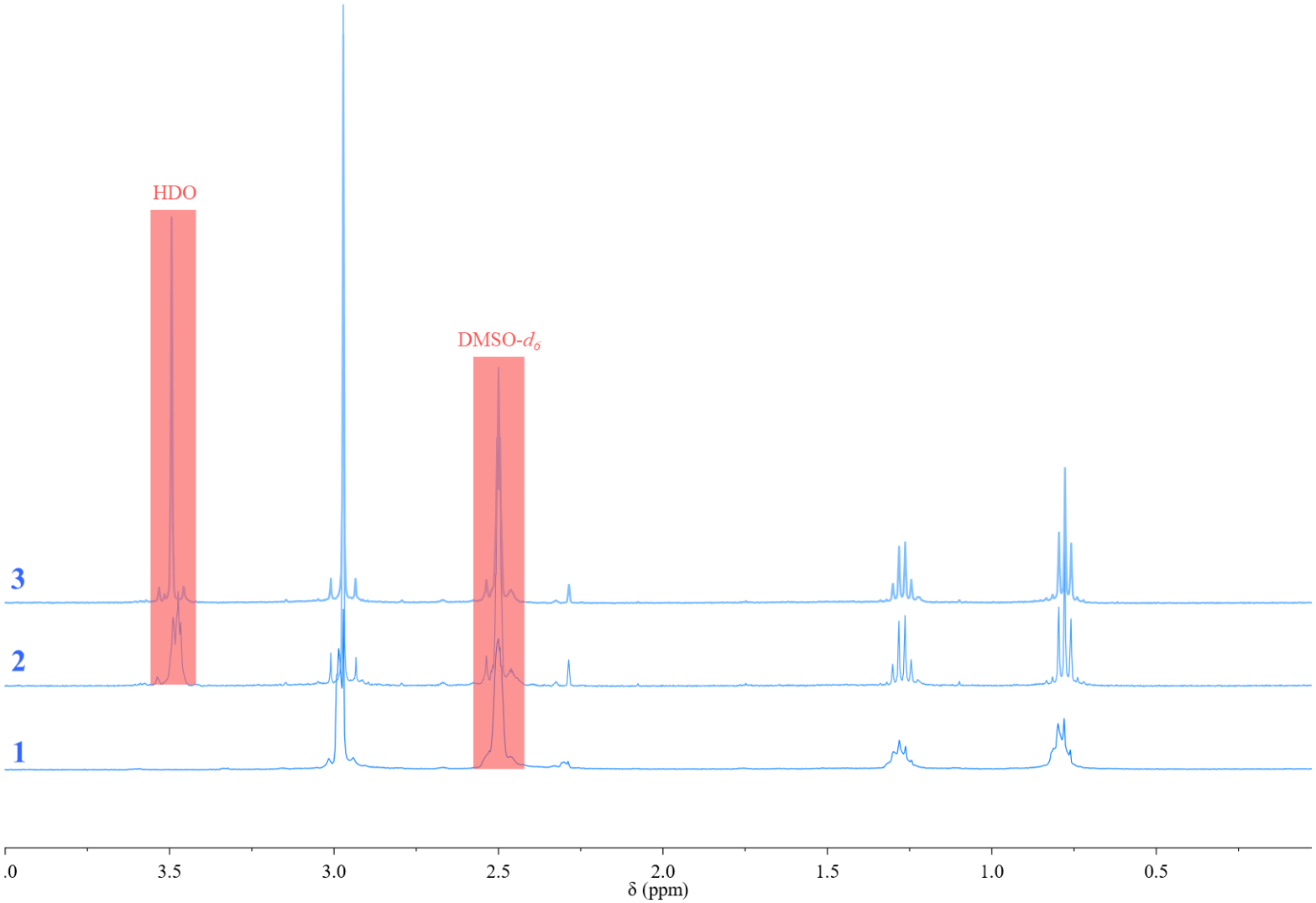

Fig. S8. Hydrolytic stability test: ^{1}H NMR of Sb-**1**$_{Et}$ (1) in dry DMSO-*d6*, (2) after addition of 10 eq of D_2O to (1), and (3) 24 hours after first data acquisition on (2).

S2.2 $^{13}C\{^{1}H\}$ NMR

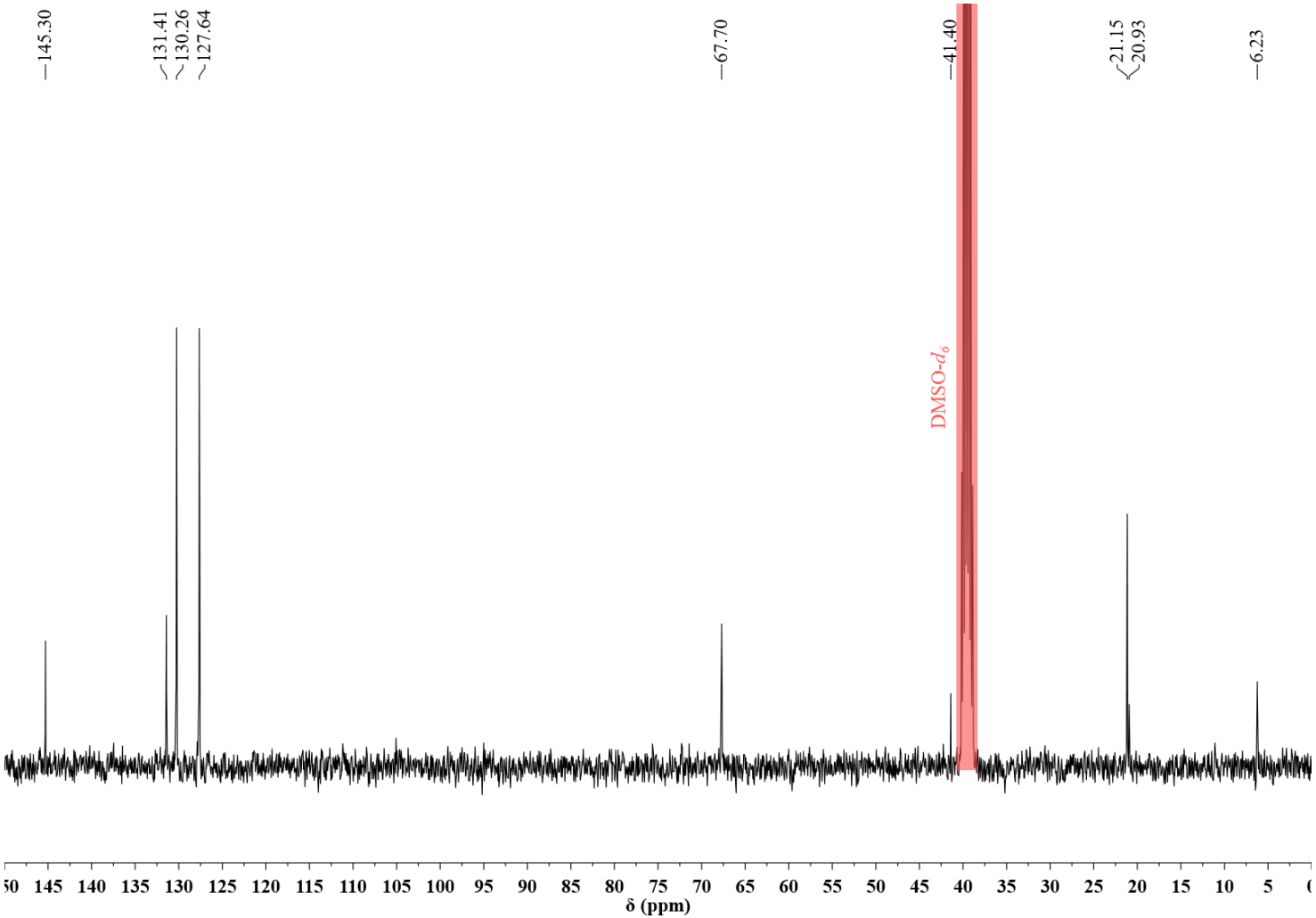

Fig. S9. $^{13}C\{^{1}H\}$ NMR of **3** in DMSO-*d6*.

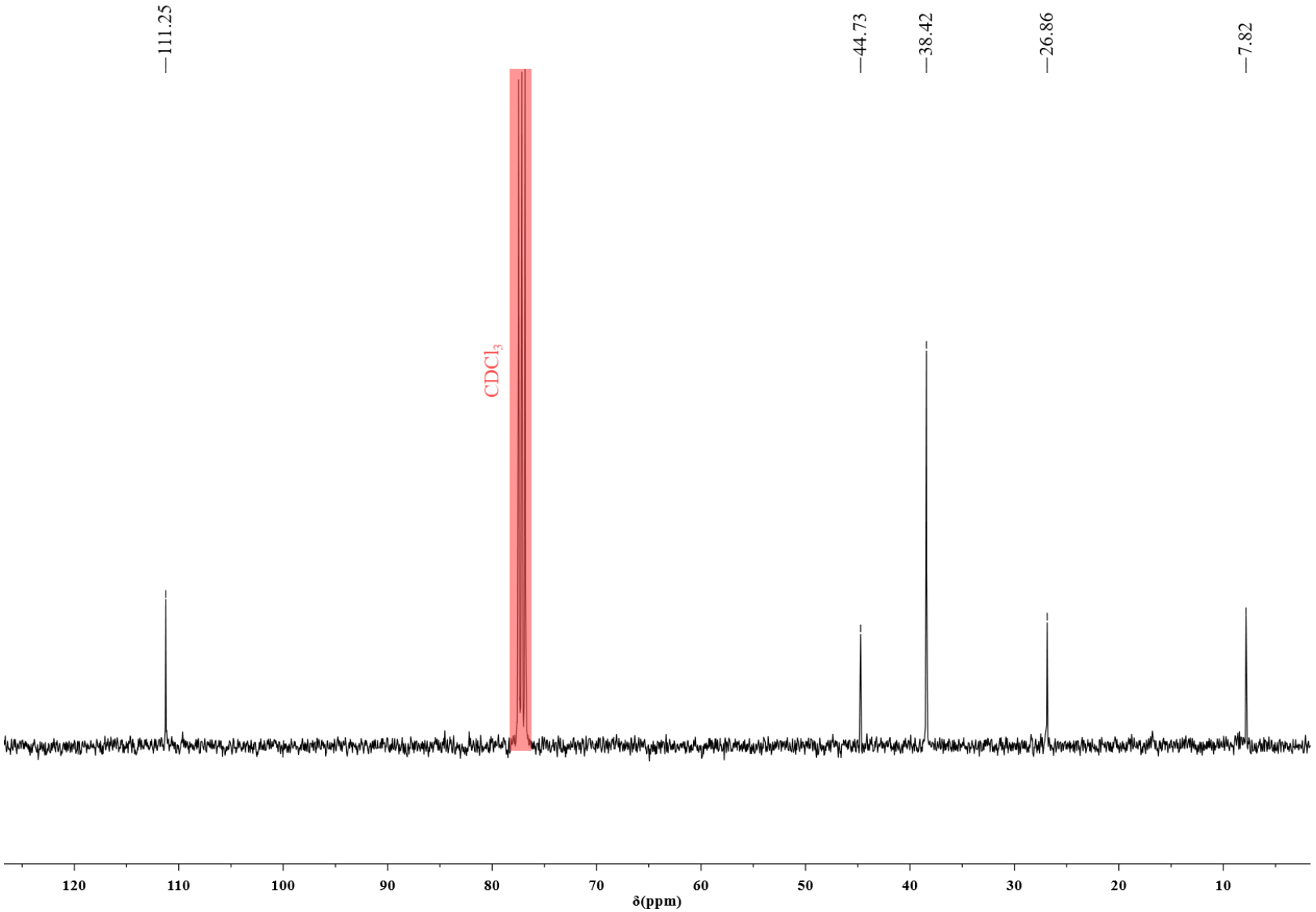

Fig. S10. $^{13}C\{^{1}H\}$ NMR of **4** in $CDCl_3$.

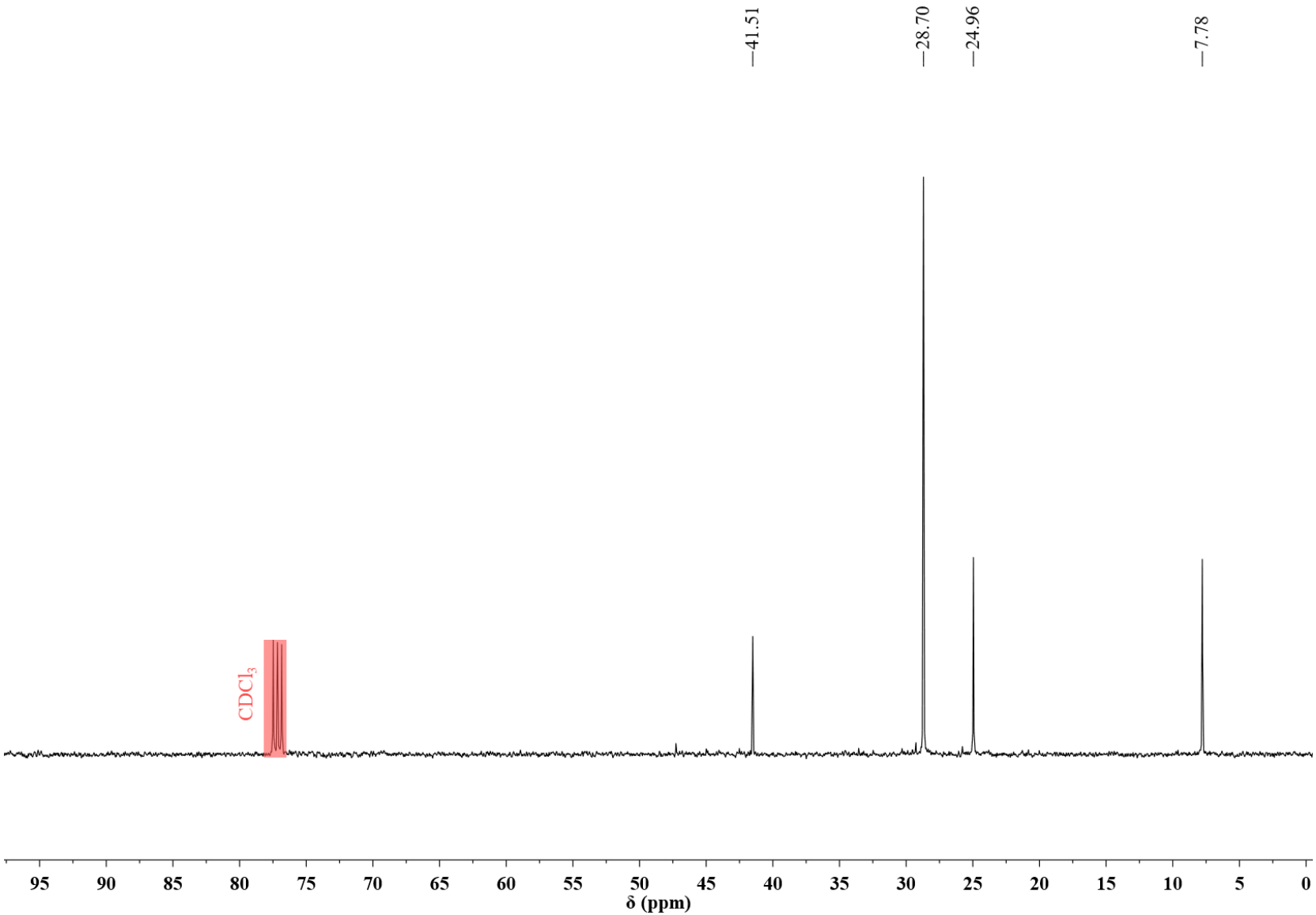

Fig. S11. $^{13}C\{^{1}H\}$ NMR of $H_3\mathbf{1}_{Et}$ in $CDCl_3$.

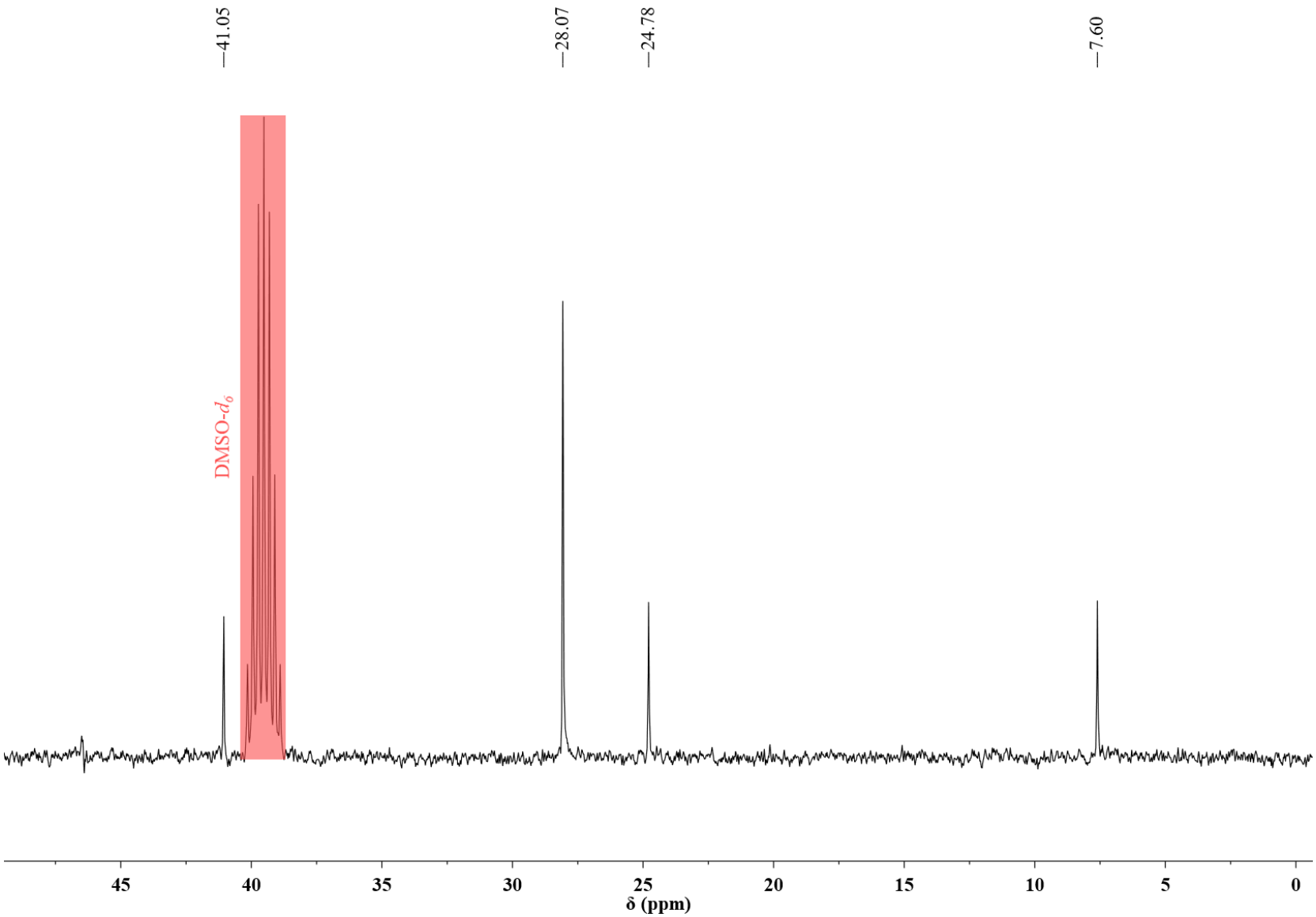

Fig. S12. $^{13}C\{^{1}H\}$ NMR of $H_3\mathbf{1}_{Et}$ in DMSO-*d6*.

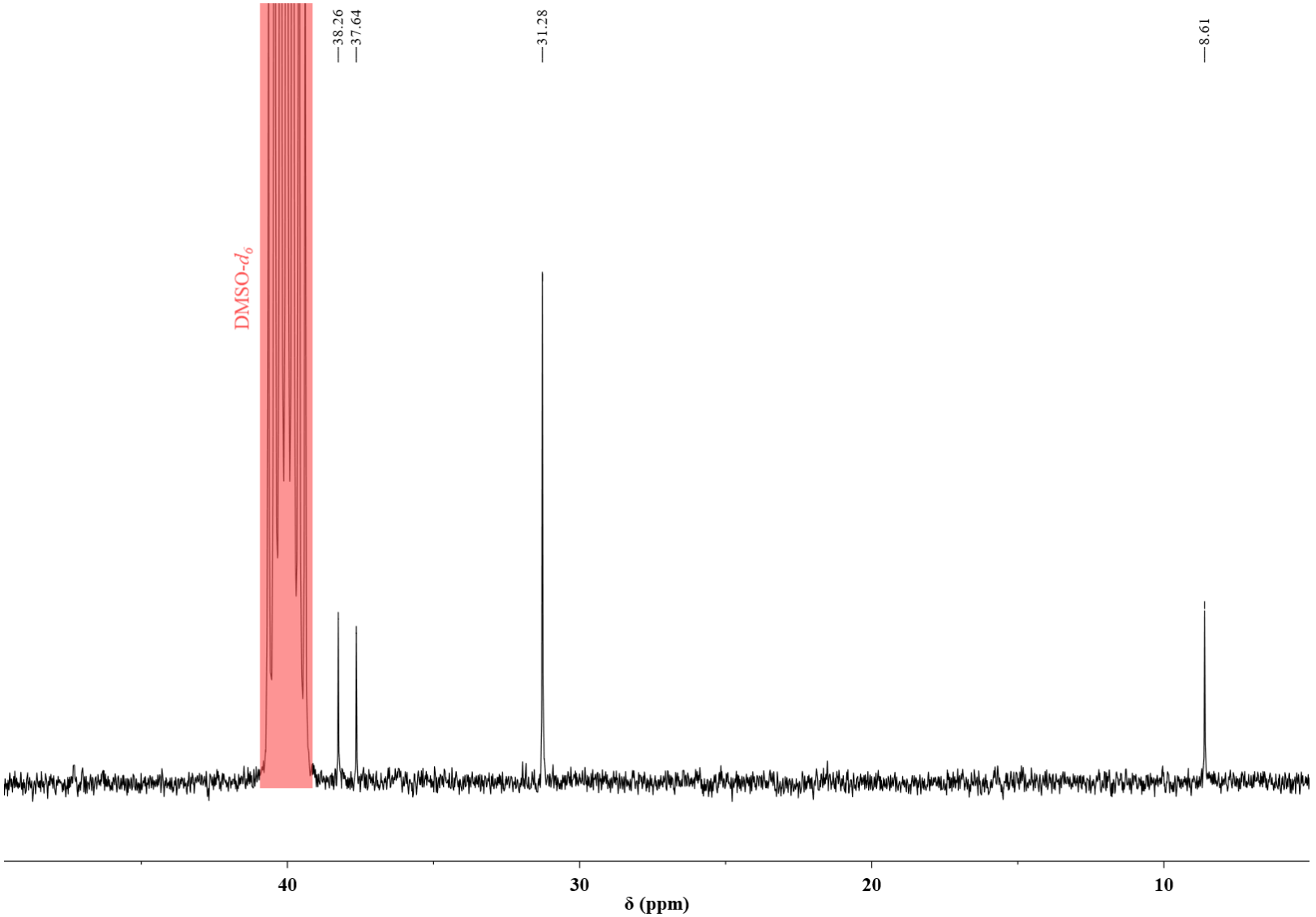

Fig. S13. $^{13}C\{^{1}H\}$ NMR of Sb-$\mathbf{1}_{Et}$ in DMSO-*d6* at 60 °C.

S2.3 FTIR

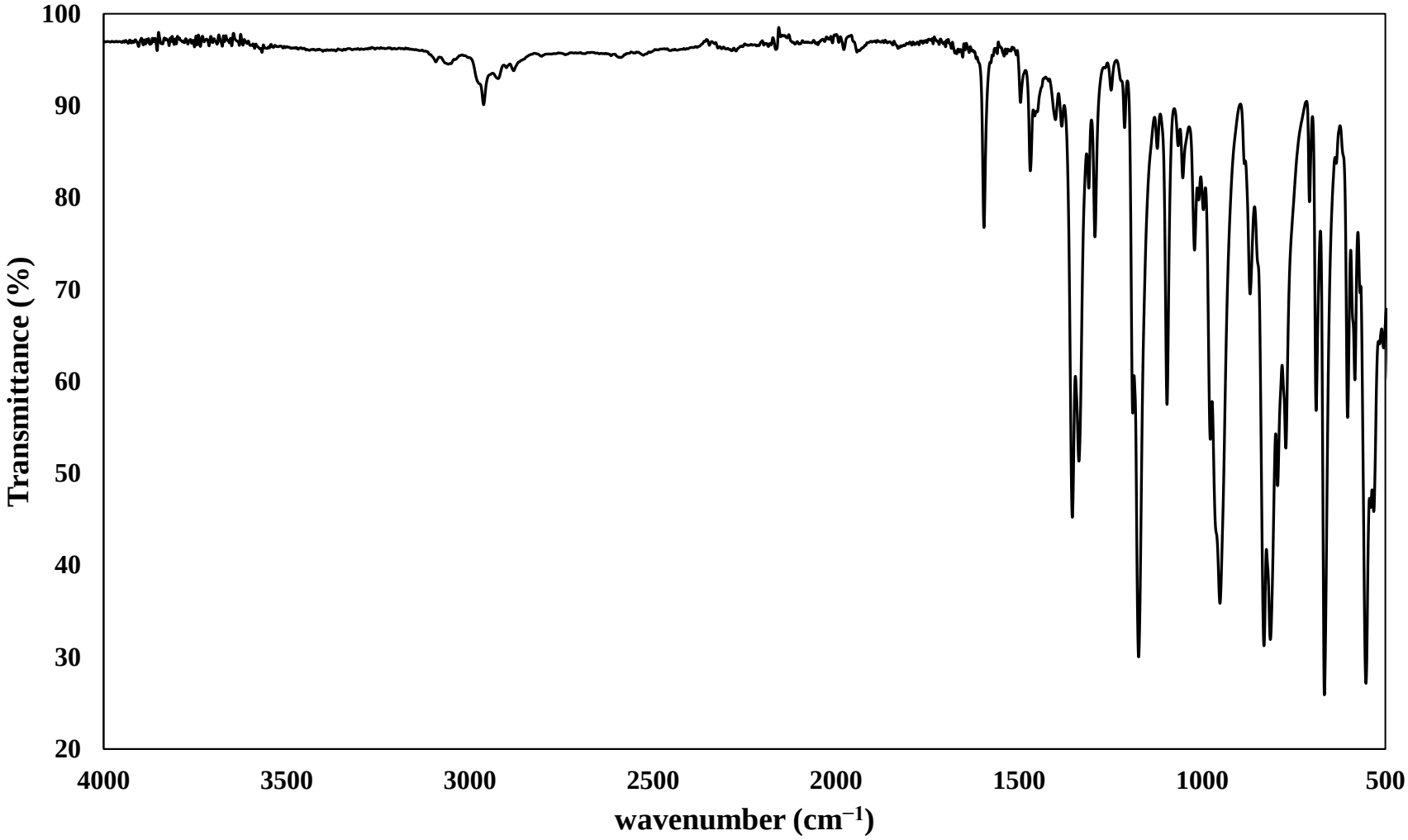

Fig. S14. Di-ATR-FTIR of **3**.

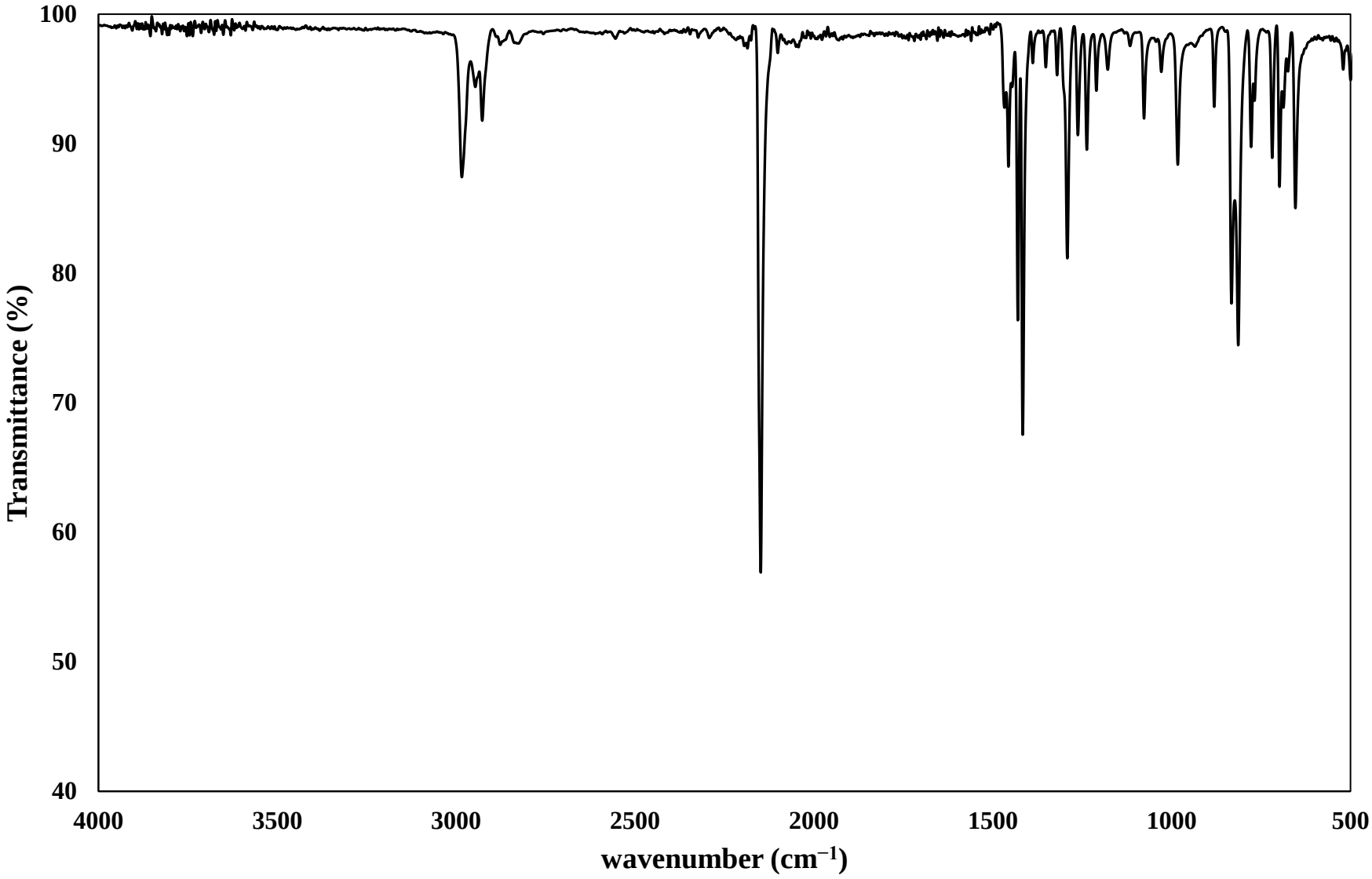

Fig. S15. Di-ATR-FTIR of **4**.

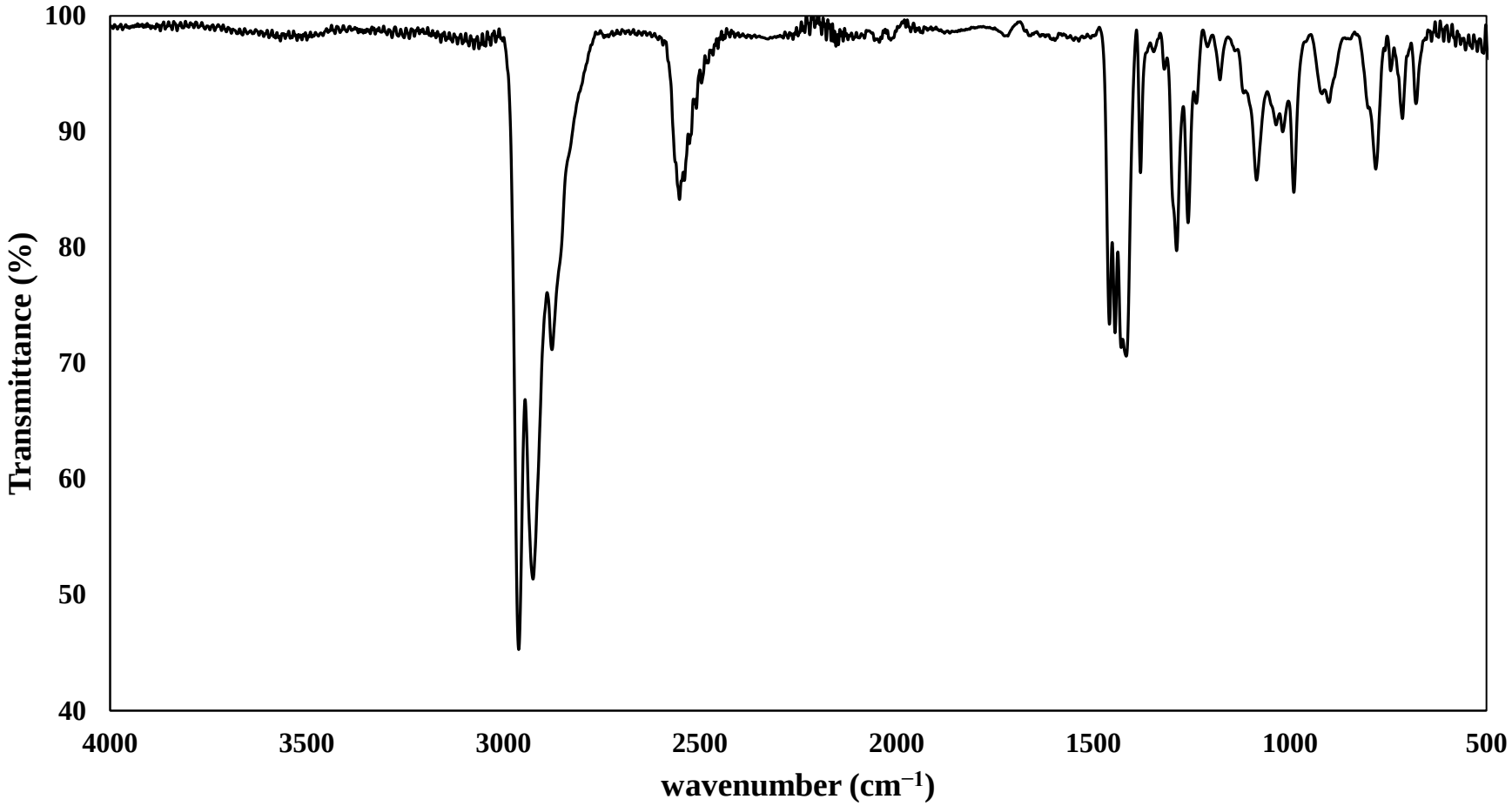

Fig. S16. Di-ATR-FTIR of $H_3\mathbf{1}_{Et}$.

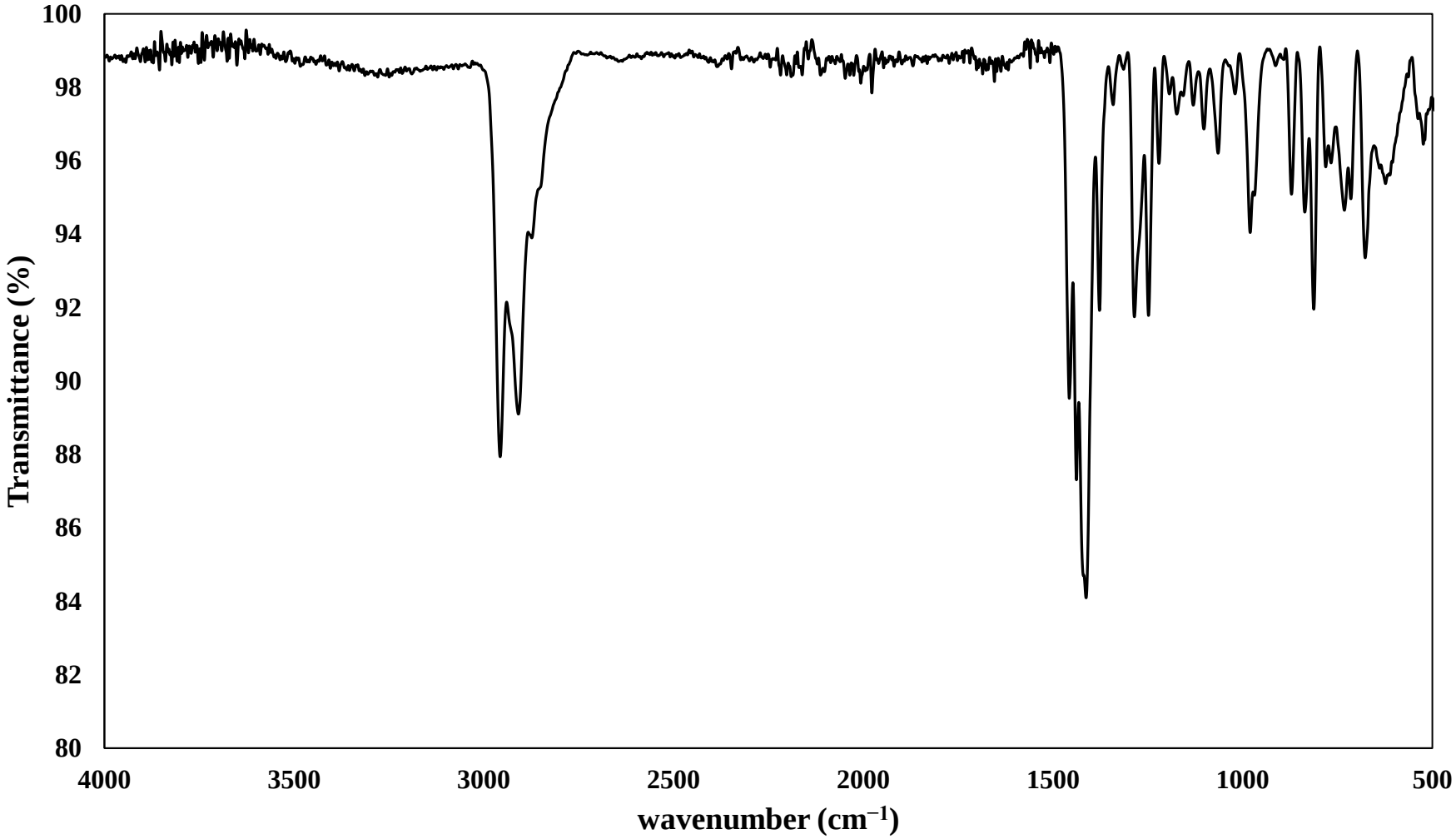

Fig. S17. Di-ATR-FTIR of Sb-$\mathbf{1}_{Et}$.

S3 Dynamic Light Scattering (DLS) Results

S3.1 Solvent choice and solution concentration

Acetone, hexanes and an acetone/hexanes (0.64:0.36 molar ratio) mixture were used to evaluate the effect of the solvent polarity and solution concentration at 40% probe power amplitude. For the hexanes solution, except for the lowest concentration (0.05 mM) for 5 minutes sonication time (Fig. S18), all concentrations show very broad and nonuniform size distribution of the particles. On the other hand, acetone solutions for all concentrations and sonication times (2 and 5 minutes) resulted in more uniform and average particle size of 100-1000 nm (Fig. S18-Fig. S21). Results from hexanes study suggested that size of vesilces could increase. As a result, a mixture of hexanes and acetone with the molar fractions of 0.36 and 0.64 respectively was used to study the effect of the solvent mixture. The same experiments were performed on the acetone/hexanes solution mixture at same power amplitude and sonication time. It appeared decreasing polarity of the solution mixture does not affect the size distribution of the vesicles which were very close to those of acetone solution (Fig. S18-Fig. S21).

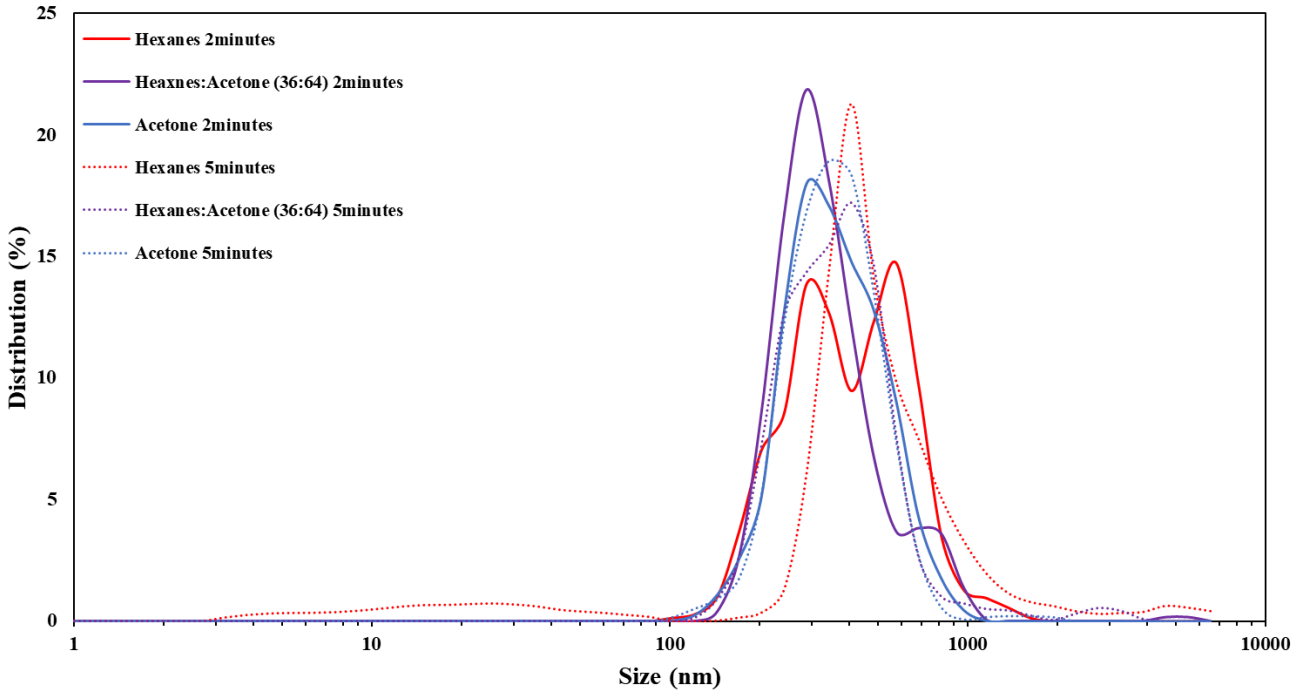

Fig. S18. Effect of solvent on the size distribution of the vesicles in 0.05 mM solutions.

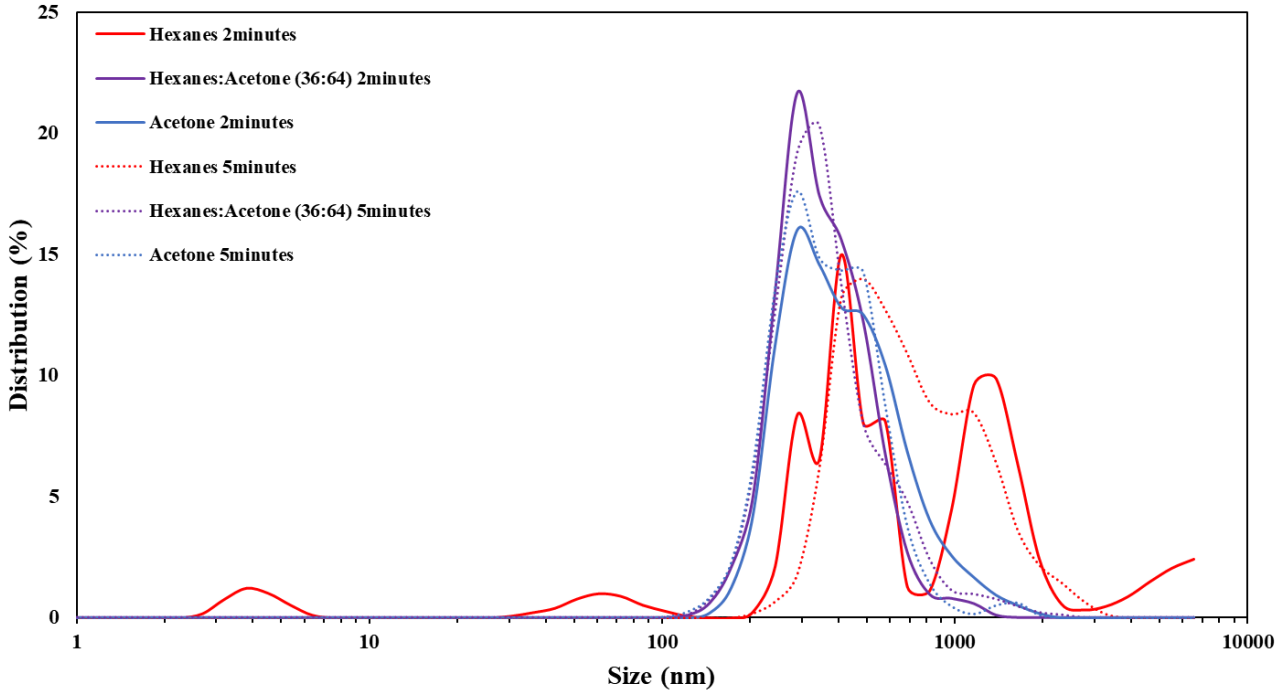

Fig. S19. Effect of solvent on the size distribution of the vesicles in 0.10 mM solutions.

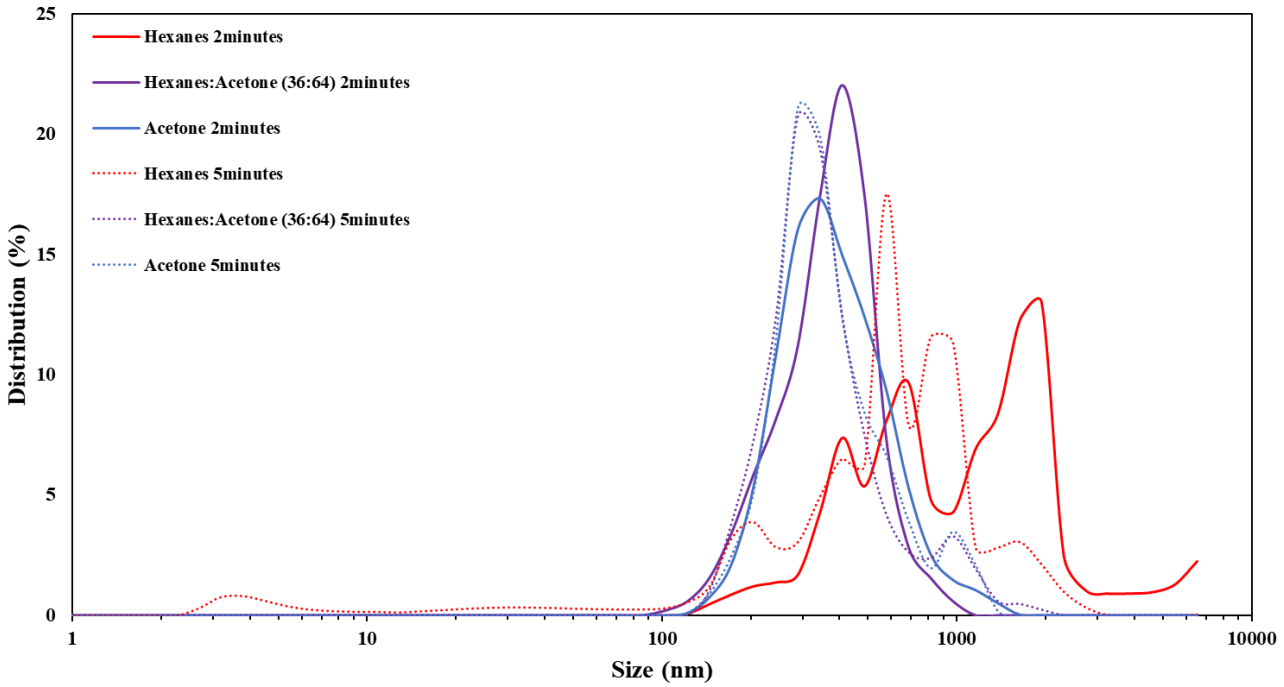

Fig. S20. Effect of solvent on the size distribution of the vesicles in 0.25 mM solutions.

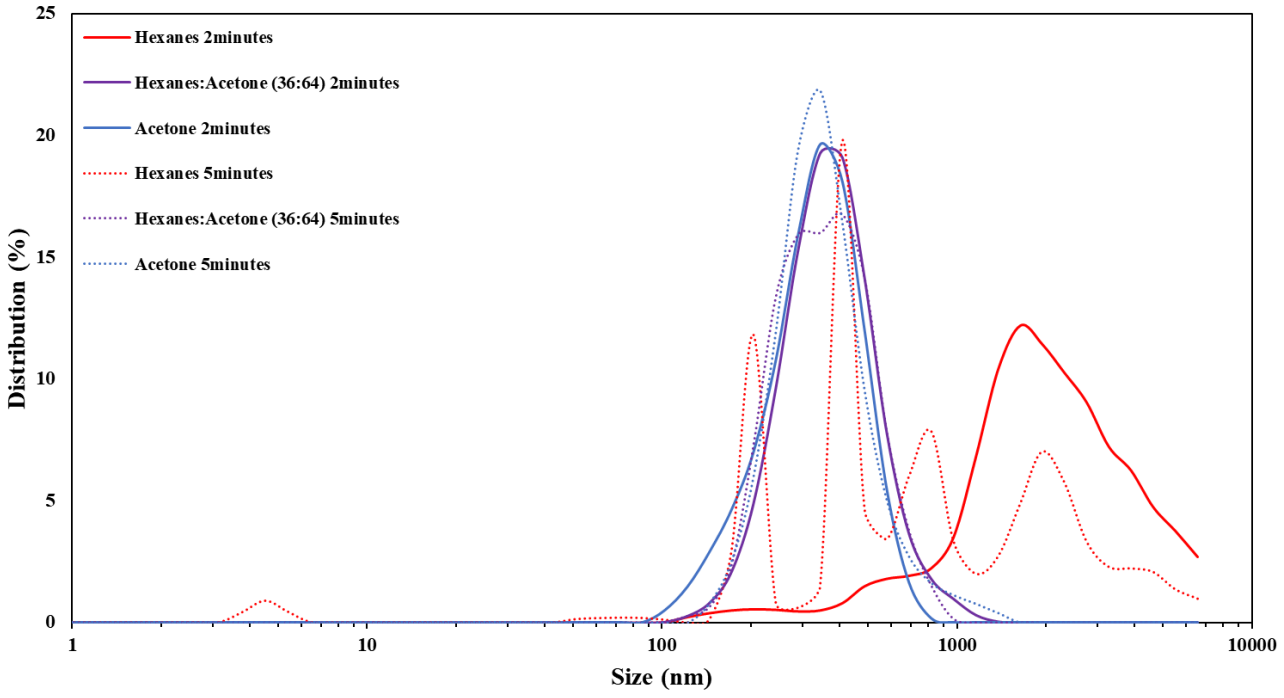

Fig. S21. Effect of solvent on the size distribution of the vesicles in 0.50 mM solutions.

S3.2 Effect of sonication time on size distribution of vesicles

Varying the sonication time from 2 to 5 and 10 minutes at 40% power amplitude, resulted in similar size distributions. This was consistent for all different concentrations as well (Fig. S22-Fig. S25).

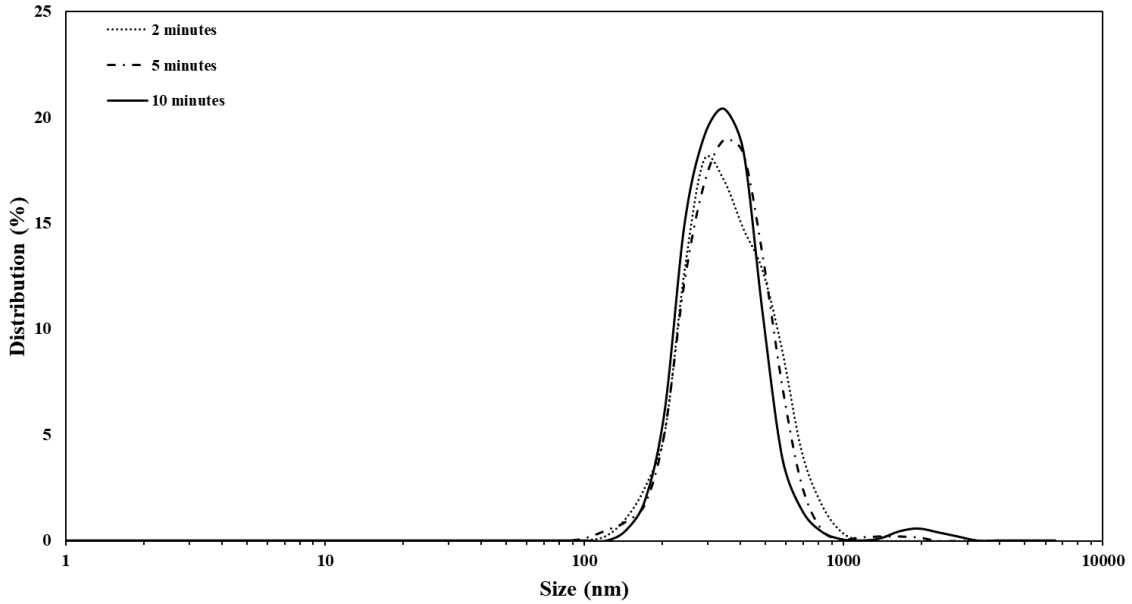

Fig. S22. Effect of time variation on the size distribution of the vesicles in 0.05 mM acetone solution.

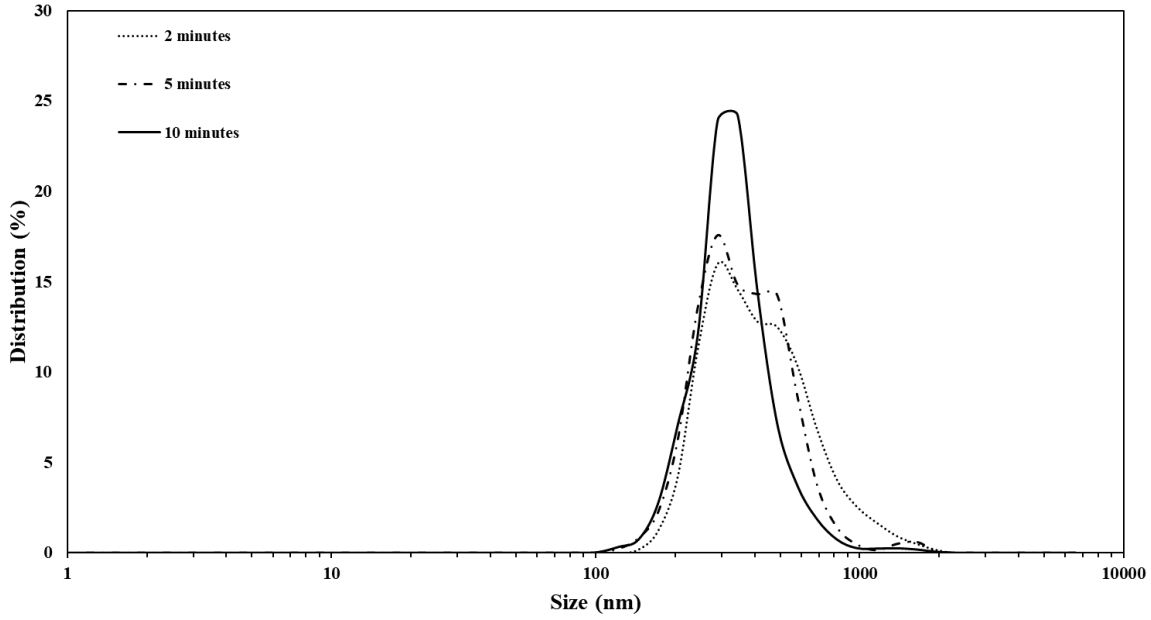

Fig. S23. Effect of time variation on the size distribution of the vesicles in 0.10 mM acetone solution.

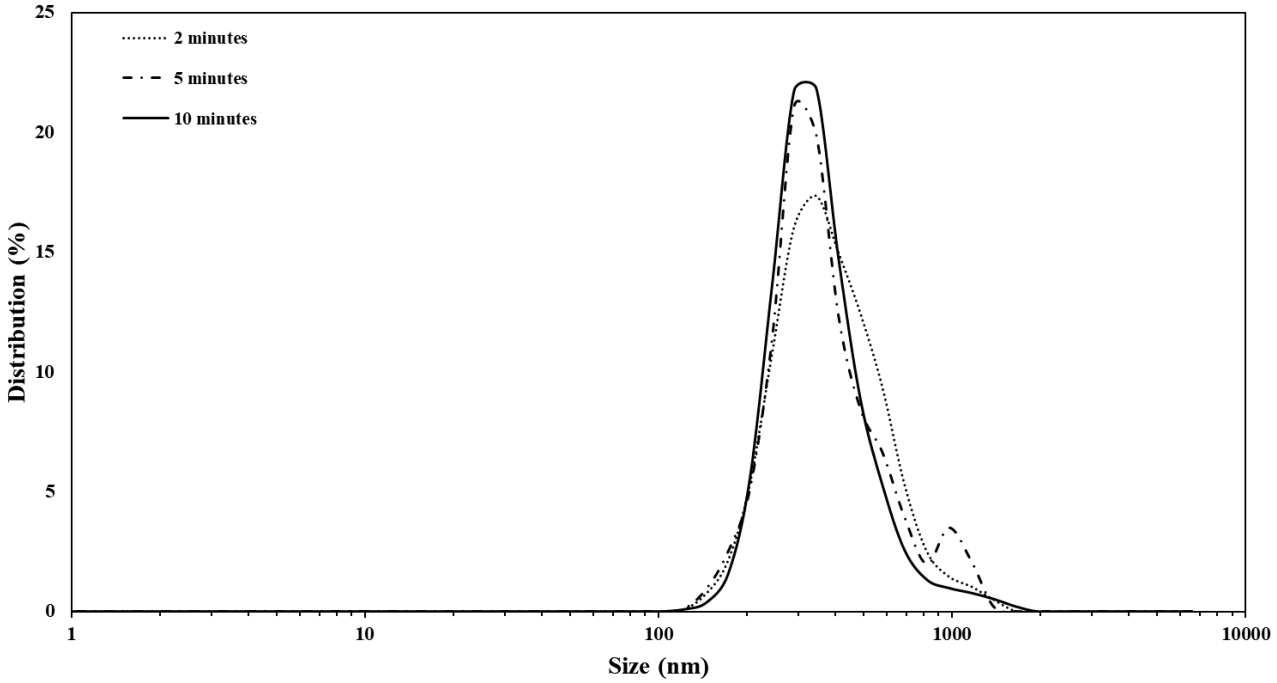

Fig. S24. Effect of time variation on the size distribution of the vesicles in 0.25 mM acetone solution.

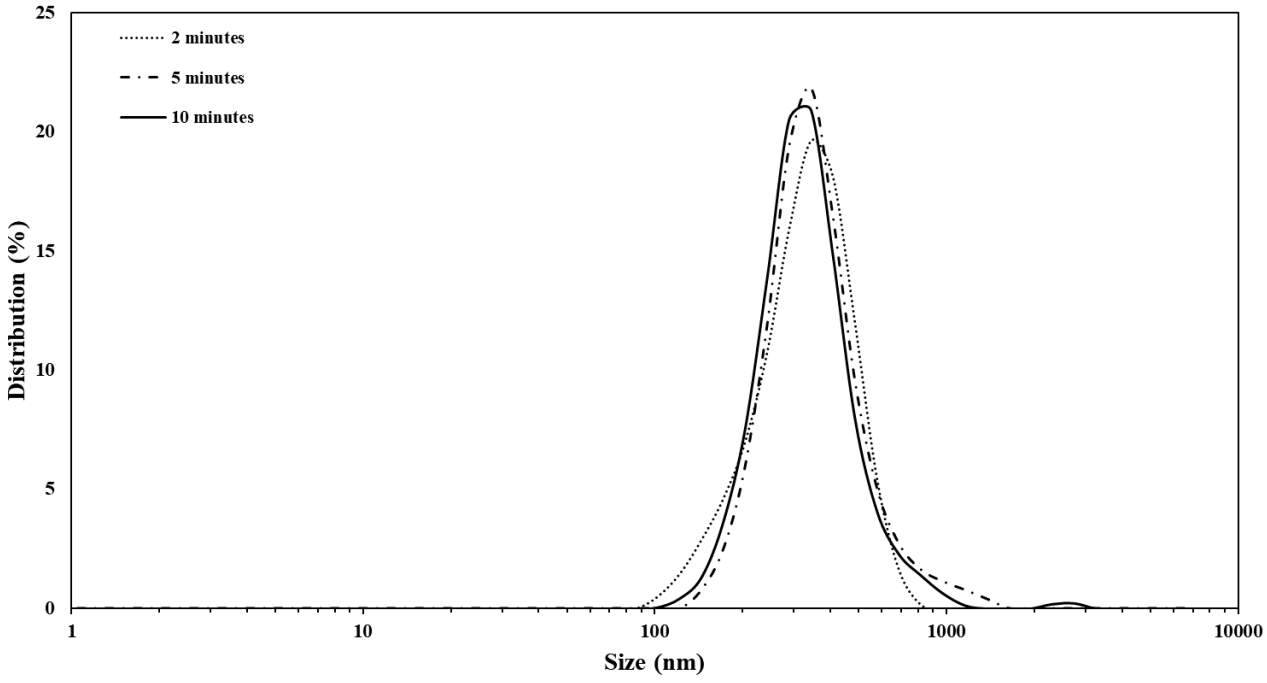

Fig. S25. Effect of time variation on the size distribution of the vesicles in 0.50 mM acetone solution.

S3.3 Effect of sonication probe power amplitude on size distribution of vesicles

Power that the ultrasonication probe can deliver during each pulse to the solution can be adjusted as well. To probe the effect of power variation, all different concentrations in acetone solution were sonicated for 5 minutes under 20%, 40% and 70% of the probe power (750 W). Changing the power did not have a drastic effect on the size distribution (Fig. S26-Fig. S29). As a result, 40% power amplitude was chosen for the rest of the experiments.

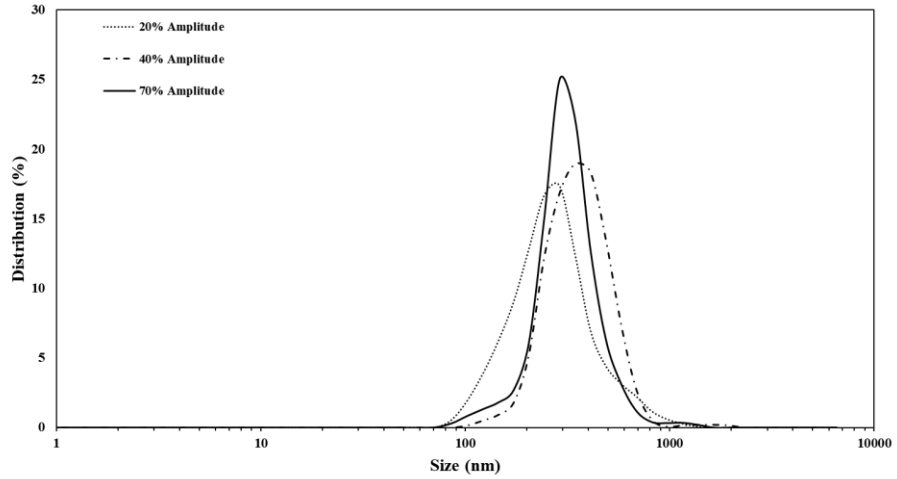

Fig. S26. Effect of sonication probe power amplitude variation on the size distribution of the vesicles in 0.05 mM acetone solution.

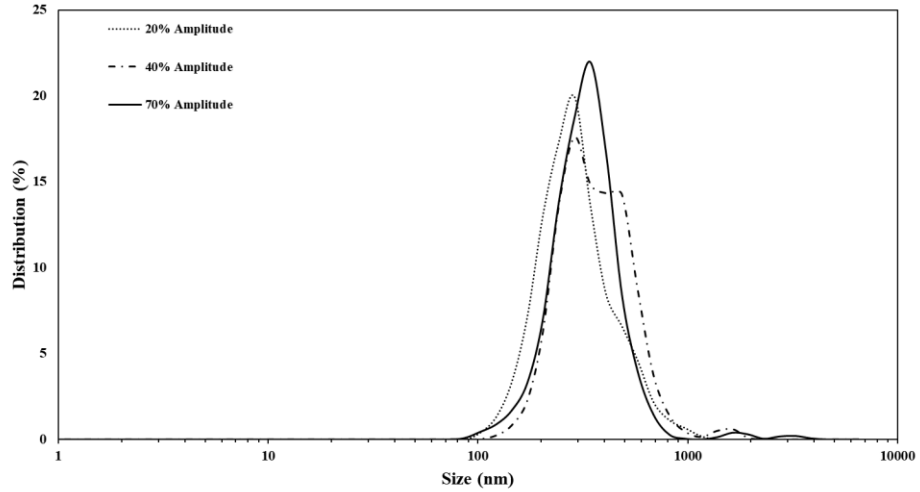

Fig. S27. Effect of sonication probe power amplitude variation on the size distribution of the vesicles in 0.10 mM acetone solution.

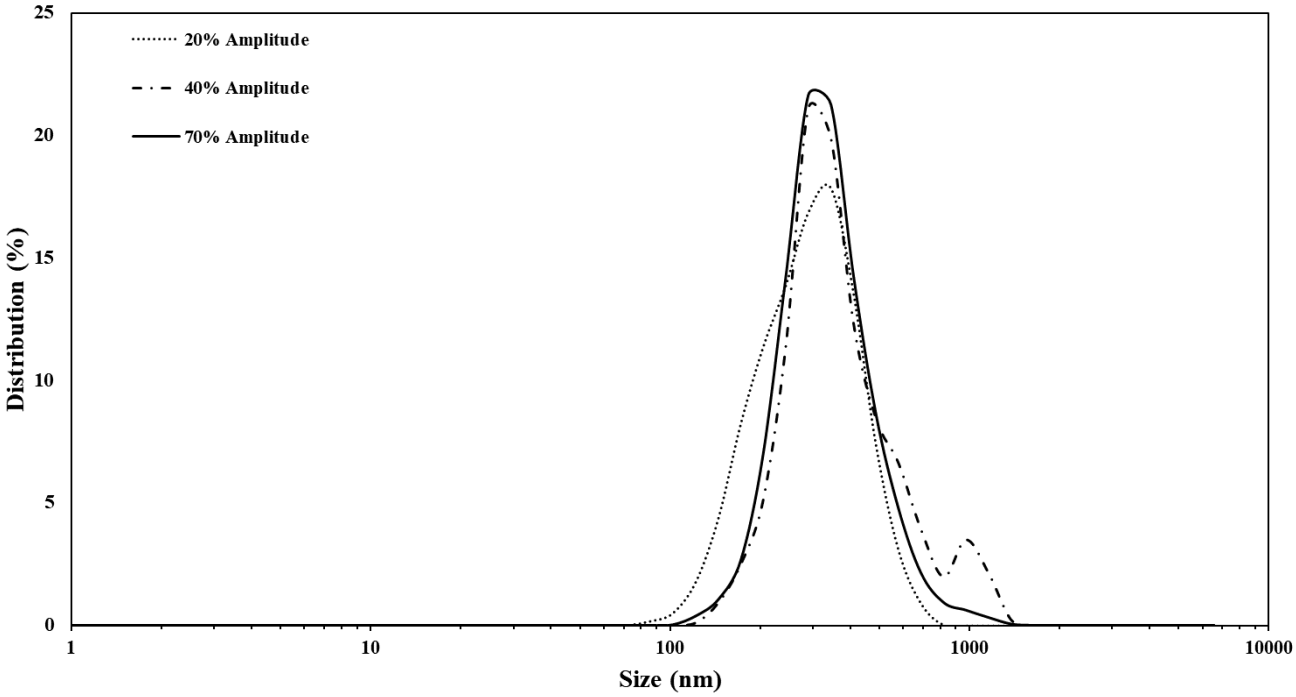

Fig. S28. Effect of sonication probe power amplitude variation on the size distribution of the vesicles in 0.25 mM acetone solution.

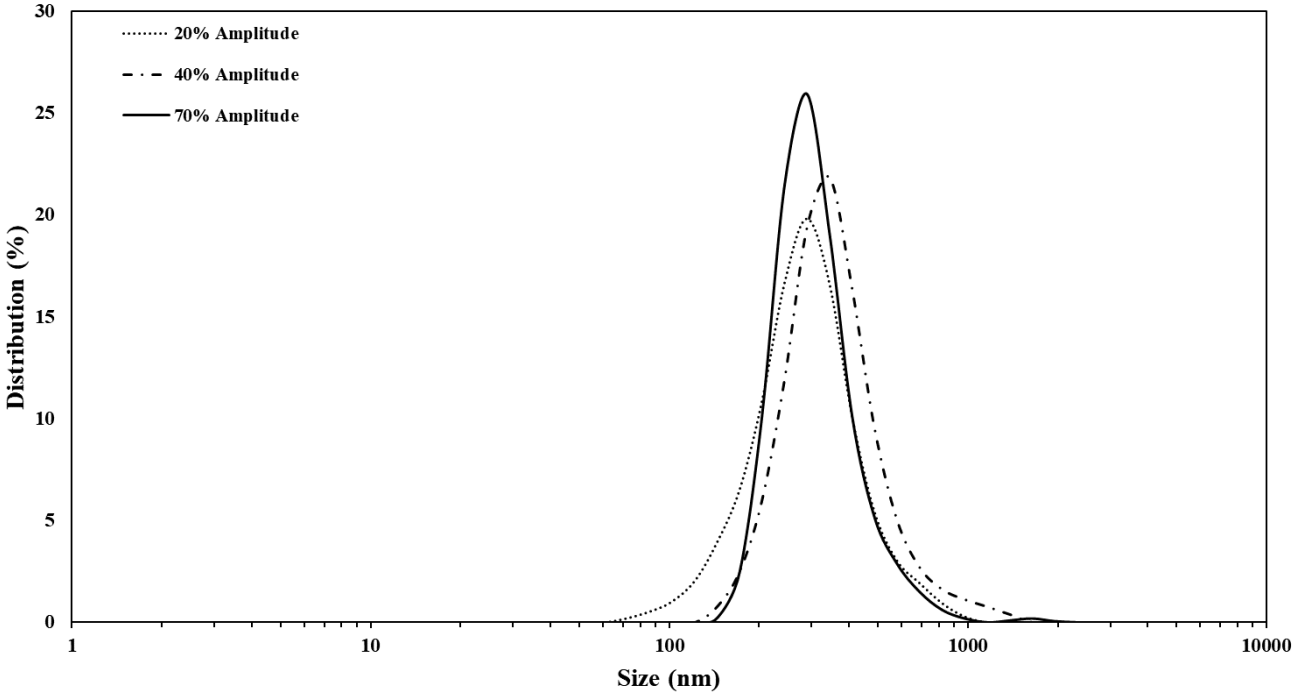

Fig. S29. Effect of sonication probe power amplitude variation on the size distribution of the vesicles in 0.50 mM acetone solution.

S4 Encapsulation Experiments

S4.1 In-situ encapsulation of ferrocene

To confirm the formation of hollow vesicles during synthesis, in-situ encapsulation of ferrocene (Fc) as a marker molecule was performed. The reaction setup was similar to preparation of Sb-$\mathbf{1}_{Et}$ in S1.2.2 where 1.5 mmol of Fc was dissolved in 20.0 mL of 0.05M hexanes solution of $H_3\mathbf{1}_{Et}$. Based on our hypothesis by adding antimony (III) *tert*-butoxide to the Fc/thiol solution, hollow vesicles must encapsulate everything that was dissolved in the reaction mixture including Fc molecules. After completion of the reaction, free Fc molecules were separated from the encapsulated ones by rinsing the vesicles with 20 mL of fresh hexanes and gently agitating the mixture before allowing the particles to settle. After the vesicles settled, the solution was decanted. This rinsing procedure was repeated 5 times. Other methods for separation of the free Fc from encapsulated molecules, such as filtration or centrifuging and resuspending (via vortex) of the vesicles, were performed and no signals of Fc or other molecules present during the reaction could be observed which suggests rupturing of them during these more aggressive purification procedures. After the rinsing steps were completed and the resulting powder was dry, DMSO-*d6* was added to a small amount the vesicles and heat was applied to the mixture, so the vesicles disassemble and release the encapsulated Fc molecules.

S4.1.1 Cyclic voltammetry of encapsulated ferrocene

Voltammetry experiments were performed in a 20 mL cell equipped with a glassy-carbon electrode (CH Instruments, Inc. CHI 104), a platinum wire auxiliary electrode, and a 0.5 mm silver wire as a pseudo-reference electrode. All measurements were performed in a 0.1 M $TBAPF_6$ chloroform solution. The electrolyte solution was scanned in a 1200 to −800 mV window to make sure that there was no redox response from the solution. All reported potentials are relative to the Fc/Fc^+

redox couple. To confirm that vesicles can form in the electrolyte solution and their integrity will remain during the dialysis process, optical microscopy images (Fig. S30) of the as-prepared and dialyzed samples were captured before and after dialysis. Samples were transferred into a capillary tube (25 mm inner diameter) and images were captured via an upright Olympus CX31 microscope with a 40×, 0.65 NA dry objective.

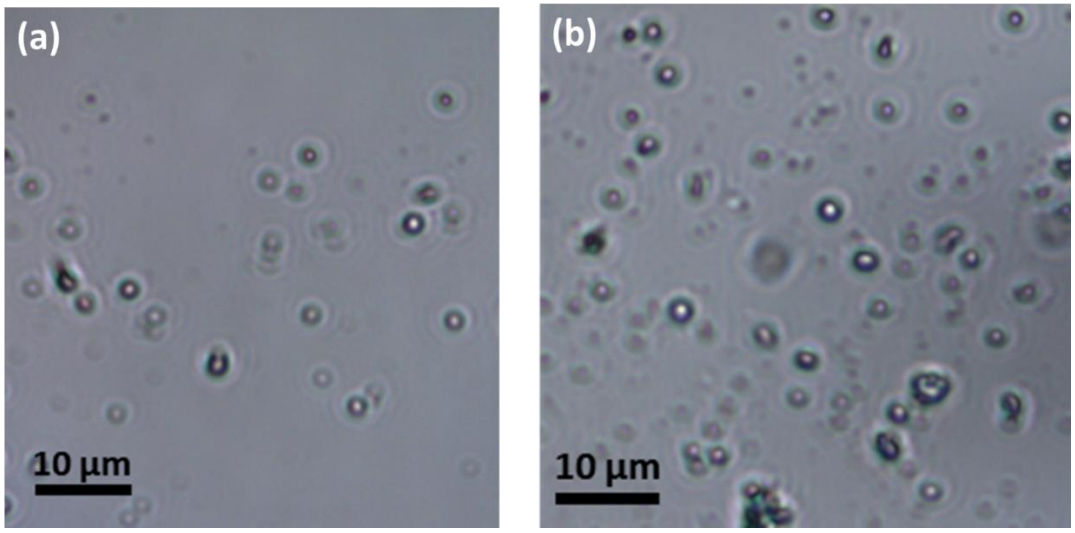

Fig. S30. Optical microscopy images of the 0.25 mM Sb-$\mathbf{1}_{Et}$ vesicles prepared in a chloroform solution of Fc (1.6 mM), and 0.1 M $TBAPF_6$. (a) Before and (b) after dialysis.

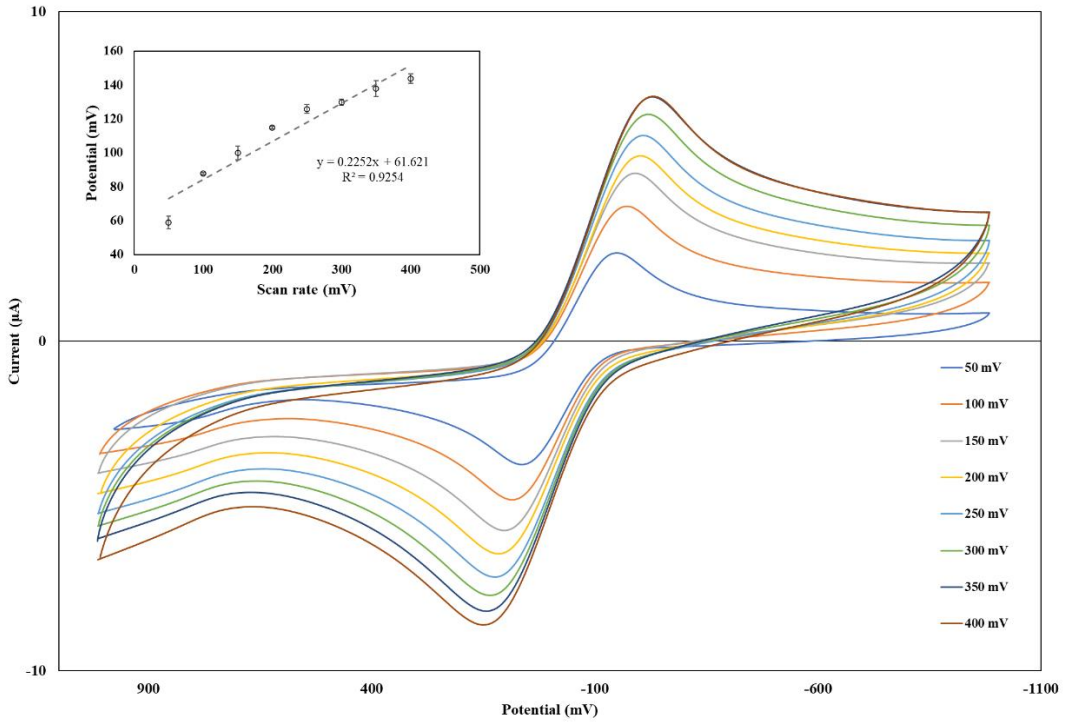

Fig. S31. CV response on glassy carbon of encapsulated Fc in 0.1 M $TBAPF_6$ in chloroform at eight different scan rates relative to Fc/Fc^+ redox couple. Inset shows the oxidation potential of Fc at each scan rate.

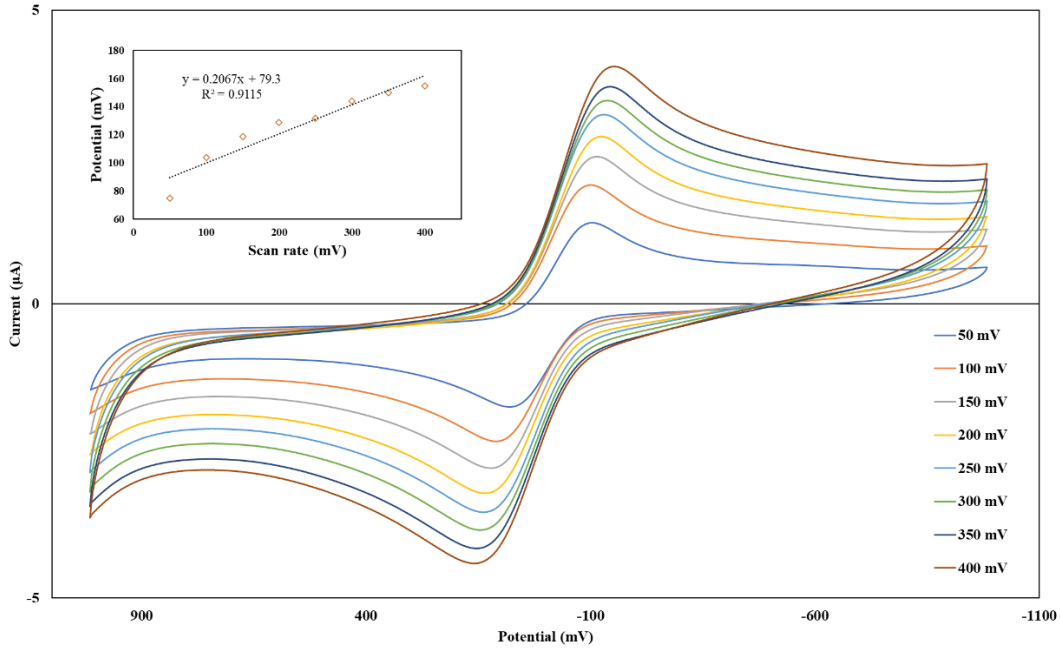

Fig. S32. CV response on glassy carbon of 0.15 mM Fc in 0.1 M $TBAPF_6$ in chloroform at eight different scan rates relative to Fc/Fc^+ redox couple. Inset shows the oxidation potential of Fc at each scan rate.

After all encapsulated samples were studied by CV analysis, a small amount of Fc was added to the encapsulated Fc sample.

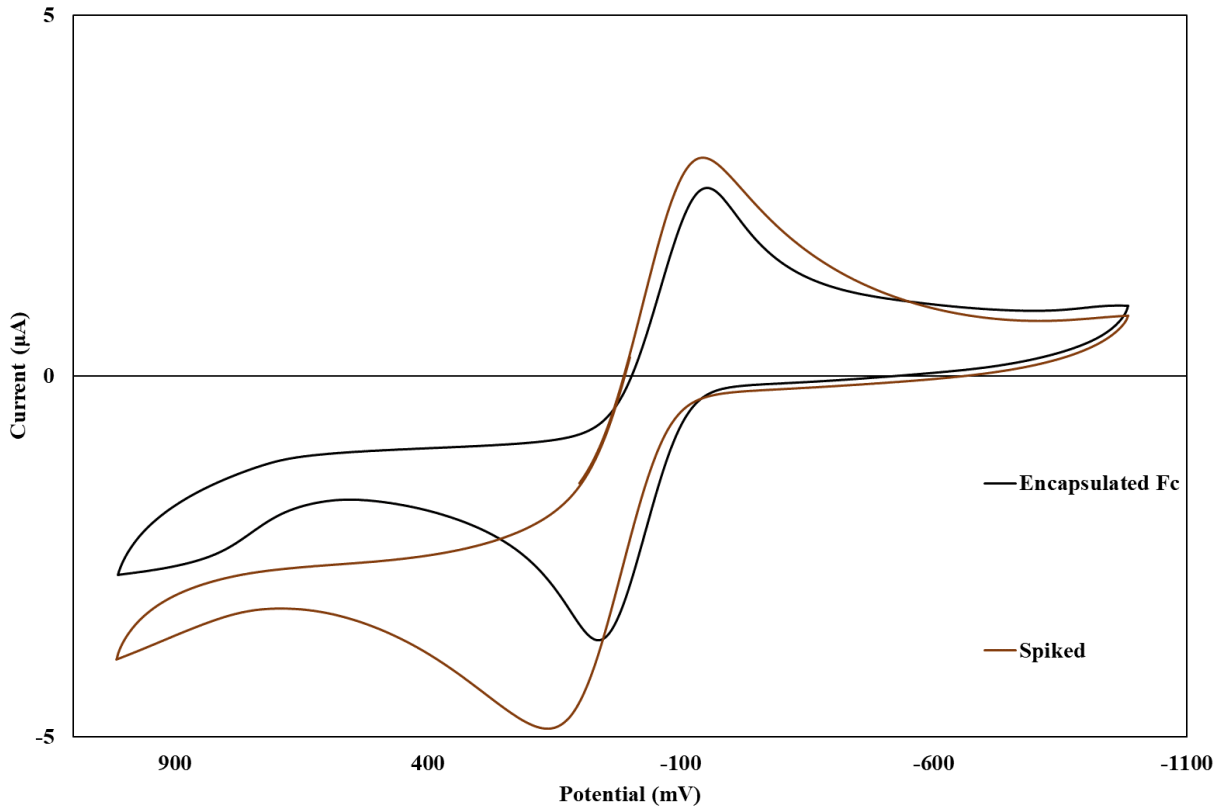

Fig. S33. CV response on glassy carbon of encapsulated Fc (black) and encapsulated Fc after being spiked with unencapsulated Fc (dark red) in 0.1 M $TBAPF_6$ in chloroform at 50 mV scan rate relative to Fc/Fc^+ redox couple.

S4.2 Encapsulation of fluorescent dyes

S4.2.1 Rhodamine B (RhB) fluorescent dye

In a 40 mL scintillation vial 1.5 mg of Sb-$\mathbf{1}_{Et}$ and ~1 mg of rhodamine B dye (RhB) were measured. Acetone (20.0 mL) was added to the solids and then the mixture was sonicated for 5 minutes at 40% power amplitude in an ice-water bath. The sonicated mixture was transferred into a dialysis bag (Spectra/Pro, 6-8kD), and the closed bag was dialyzed in 1.4 L of acetone for 48 hours. During

the dialysis process the dialysis solvent was replaced with fresh acetone (1.4 L) two times.

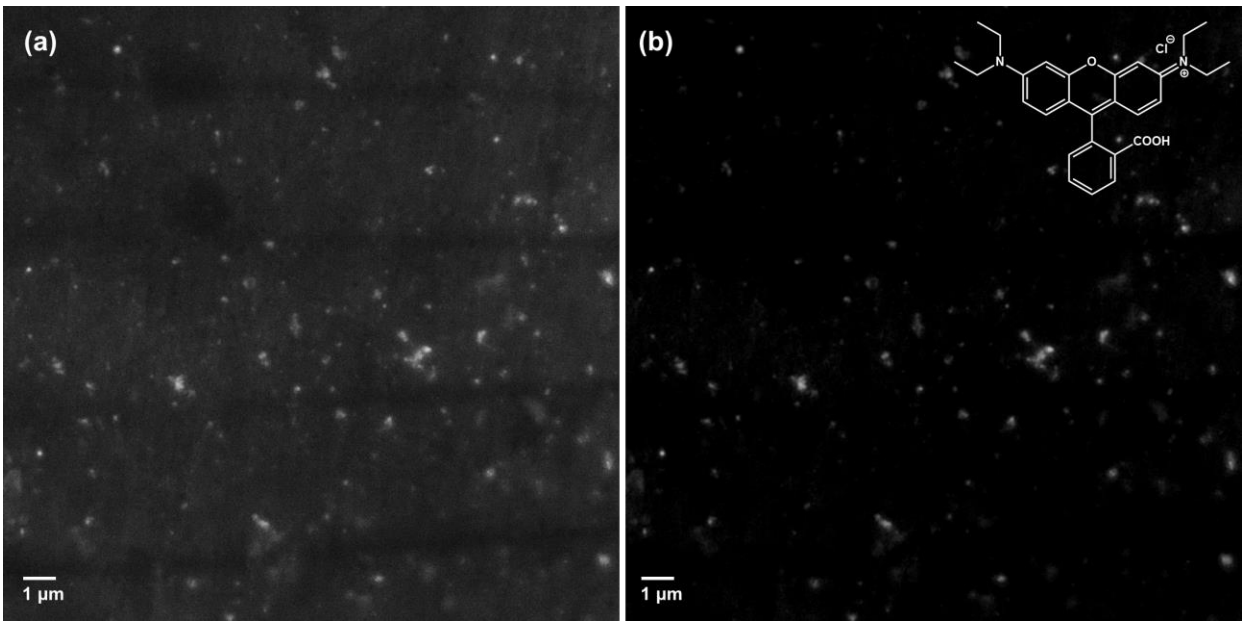

Fig. S34. Fluorescence microscopy images of the encapsulated RhB dye after dialysis. (a) raw image and (b) enhanced contrast image.

After image collection, a drop of waster was cast on the

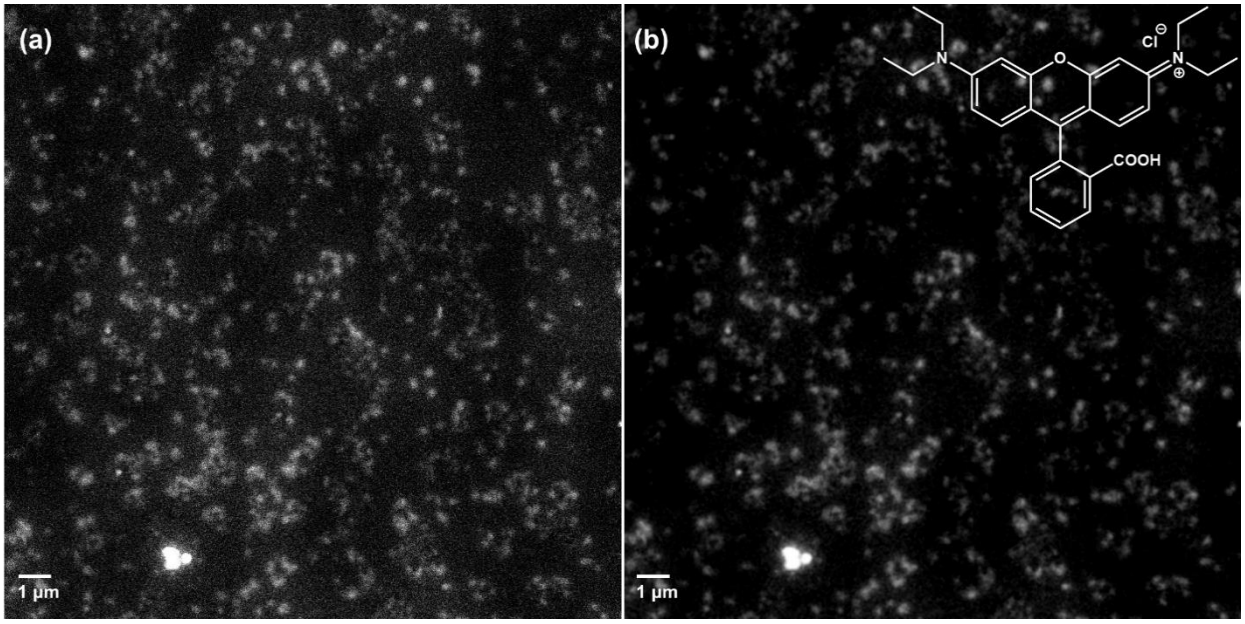

Fig. S35. Fluorescence microscopy images of the encapsulated RhB dye after 3 months storage in solution state. (a) raw image and (b) enhanced contrast image.

S4.2.2 6-Carboxyfluorescein (6-FAM)

1.5 mg of Sb-$\mathbf{1}_{Et}$ and 1.5 mg of 6-caboxyfluorescein dye (6-FAM) were measured into a 40 mL scintillation vial. Acetone (20.0 mL) was added to the solids and then the mixture was sonicated for 5 minutes at 40% power amplitude in an ice-water bath. The sonicated mixture was transferred into a dialysis bag (Spectra/Pro, 6-8kD), and the closed bag was dialyzed in 1.4 L of acetone for 48 hours. During the dialysis process the dialysis solvent was replaced with fresh acetone (1.4 L) two times.

Following dialysis, a drop of the dialyzed solution was cast on a glass slide. In a dark room, microscopy images of the vesicles were captured under white light and fluorescence images were capture under exposure to blue light before and after exposing the vesicles to water, in order to lyse the vesicles, to confirm that the fluorescent dye was encapsulated inside the vesicles.

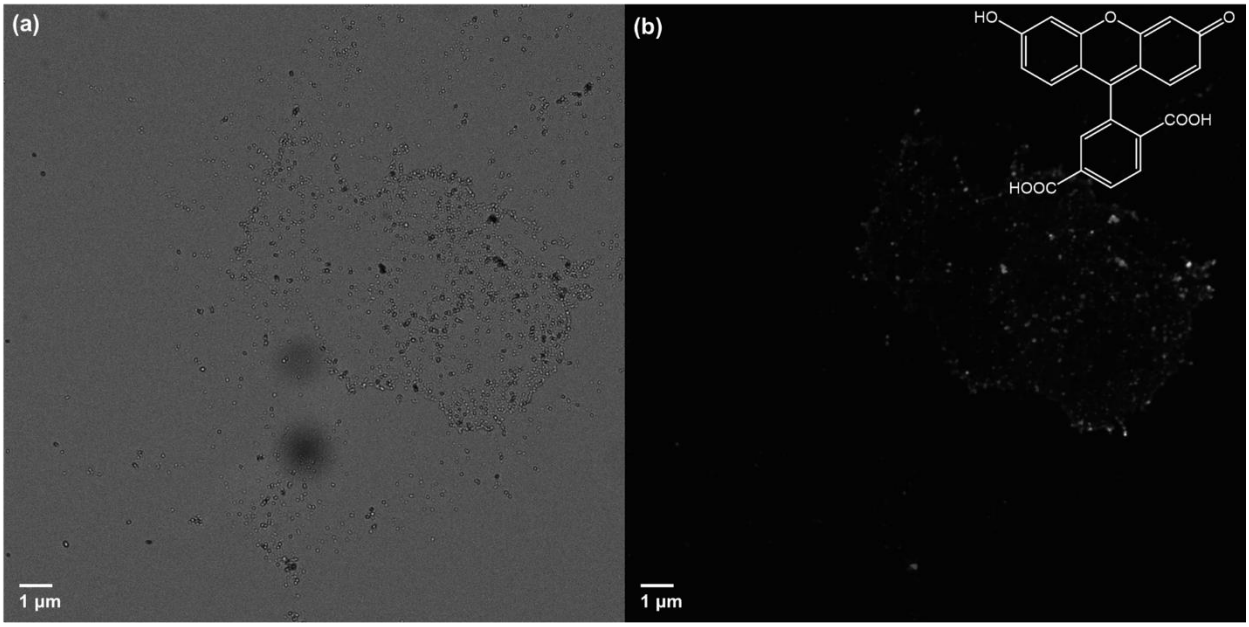

Fig. S36. Microscopy images of Sb-$\mathbf{1}_{Et}$ vesicles prepared in acetone with 6-FAM dye encapsulated inside. (a) under white light and (b) fluorescence images under blue light.

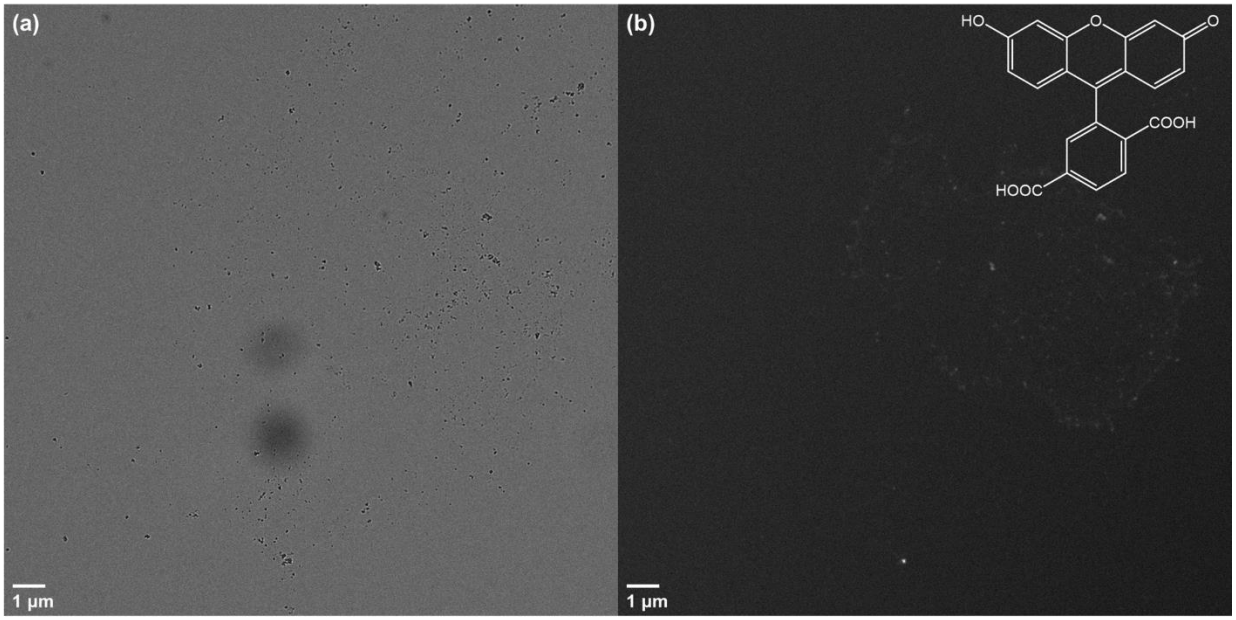

Fig. S37. Microscopy images of Lysed Sb-$\mathbf{1}_{Et}$ vesicles after exposure to water for 20 minutes. (a): under white light and (b) fluorescence images under blue light.

S4.2.3 Acridone-based fluorescent dye

In a 40 mL scintillation vial 1.5 mg of Sb-$\mathbf{1}_{Et}$ and ~0.1 mg of Acridone-based dye (Ac) was measured. Chloroform (20.0 mL) was added to the solids and then the mixture was sonicated for 5 minutes at 40% power amplitude in an ice-water bath. The sonicated mixture was transferred into a dialysis bag (Spectra/Pro, 6-8kD), and the closed bag was dialyzed in 1.4 L of chloroform for 48 hours. During the dialysis process the dialysis solvent was replaced with fresh chloroform (1.4 L) two times.

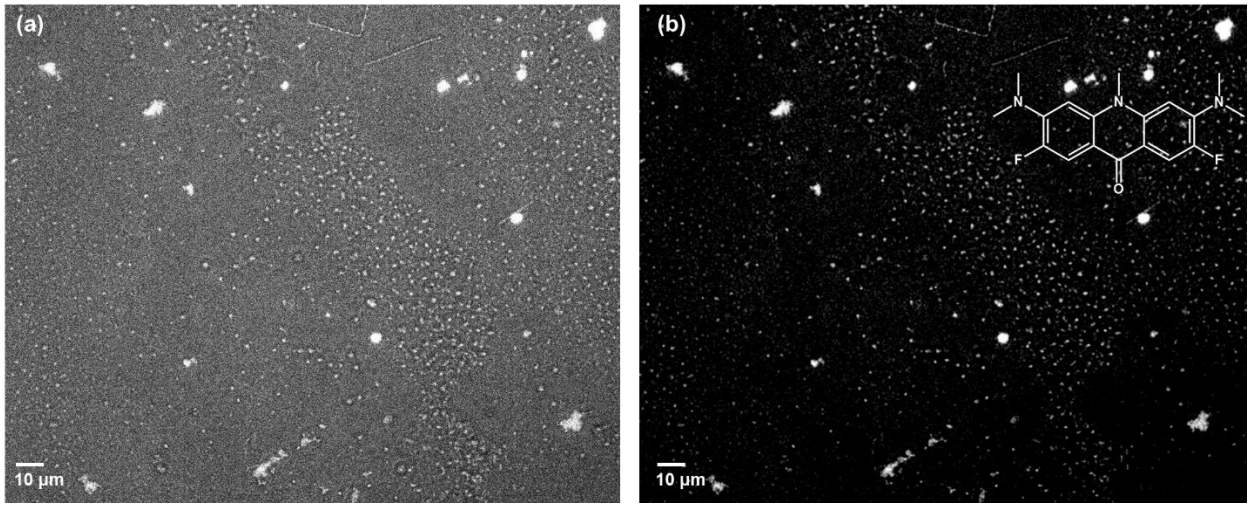

Fig. S38. Fluorescence microscopy images of the encapsulated Ac dye after 3 months storage in solution state. (a) raw image and (b) enhanced contrast image.

S5 References

(1) Moaven, S.; Yu, J.; Yasin, J.; Unruh, D. K.; Cozzolino, A. F. Precise Steric Control over 2D versus 3D Self-Assembly of Antimony(III) Alkoxide Cages through Strong Secondary Bonding Interactions. *Inorg. Chem.* **2017**, *56* (14), 8372–8380. https://doi.org/10.1021/acs.inorgchem.7b01049.

(2) Kolomyjec, C.; Whelan, J.; Bosnich, B. Biological Analogs. Synthesis of Vicinal Trimercapto Ligands. *Inorg. Chem.* **1983**, *22* (16), 2343–2345. https://doi.org/10.1021/ic00158a026.

(3) Sheldrick, G. i. SADABS, Program for Empirical Absorption Correction of Area Detector Data. *Univ. Gött. Ger.* **1996**.

(4) Sheldrick, G. M. *SHELXTL*; University of Göttingen, Germany, 2014.

(5) Sheldrick, G. M. Crystal Structure Refinement with SHELXL. *Acta Crystallogr. Sect. C Struct. Chem.* **2015**, *71* (1), 3–8. https://doi.org/10.1107/S2053229614024218.
(6) Neese, F. *ORCA – an Ab Initio, Density Functional and Semiempirical Program Package, Version 2.9.0*; Max-Planck-Insitut für Bioanorganische Chemie, Mülheim and der Ruhr, 2013.
(7) van Lenthe, E.; Baerends Evert, J.; Snijders, J. G. No Title. *J Chem Phys* **1993**, *99*, 4597–4610.
(8) Heully, J. L.; Lindgren, I.; Lindroth, E.; Lundqvist, S.; Maartensson-Pendrill, A. M. No Title. *J Phys B Mol Phys* **1986**, *19*, 2799–2815.
(9) Grimme, S.; Ehrlich, S.; Goerigk, L. Effect of the Damping Function in Dispersion Corrected Density Functional Theory. *J. Comput. Chem.* **2011**, *32* (7), 1456–1465. https://doi.org/10.1002/jcc.21759.
(10) Weigend, F.; Ahlrichs, R. Balanced Basis Sets of Split Valence, Triple Zeta Valence and Quadruple Zeta Valence Quality for H to Rn: Design and Assessment of Accuracy. *Phys. Chem. Chem. Phys.* **2005**, *7* (18), 3297–3305. https://doi.org/10.1039/B508541A.
(11) Schafer, A.; Horn, H.; Ahlrichs, R. Fully Optimized Contracted Gaussian Basis Sets for Atoms Li to Kr. *J. Chem. Phys.* **1992**, *97* (4), 2571–2577. https://doi.org/10.1063/1.463096.
(12) Weigend, F. Accurate Coulomb-Fitting Basis Sets for H to Rn. *Phys. Chem. Chem. Phys.* **2006**, *8* (9), 1057–1065. https://doi.org/10.1039/B515623H.
(13) Kohn, W.; Sham, L. J. Self-Consistent Equations Including Exchange and Correlation Effects. *Phys. Rev.* **1965**, *140* (4A), A1133–A1138. https://doi.org/10.1103/PhysRev.140.A1133.
(14) Kendall, R. A.; Früchtl, H. A. The Impact of the Resolution of the Identity Approximate Integral Method on Modern Ab Initio Algorithm Development. *Theor. Chem. Acc.* **1997**, *97* (1), 158–163. https://doi.org/10.1007/s002140050249.
(15) Boys, S. F.; Bernardi, F. The Calculation of Small Molecular Interactions by the Differences of Separate Total Energies. Some Procedures with Reduced Errors. *Mol. Phys.* **1970**, *19* (4), 553–566. https://doi.org/10.1080/00268977000101561.
(16) Lu, T.; Chen, F. Multiwfn: A Multifunctional Wavefunction Analyzer. *J. Comput. Chem.* **2012**, *33* (5), 580–592. https://doi.org/10.1002/jcc.22885.
(17) Lu, T.; Chen, F. Quantitative Analysis of Molecular Surface Based on Improved Marching Tetrahedra Algorithm. *J. Mol. Graph. Model.* **2012**, *38*, 314–323. https://doi.org/10.1016/j.jmgm.2012.07.004.
(18) Allouche, A.-R. Gabedit—A Graphical User Interface for Computational Chemistry Softwares. *J. Comput. Chem.* **2011**, *32* (1), 174–182. https://doi.org/10.1002/jcc.21600.